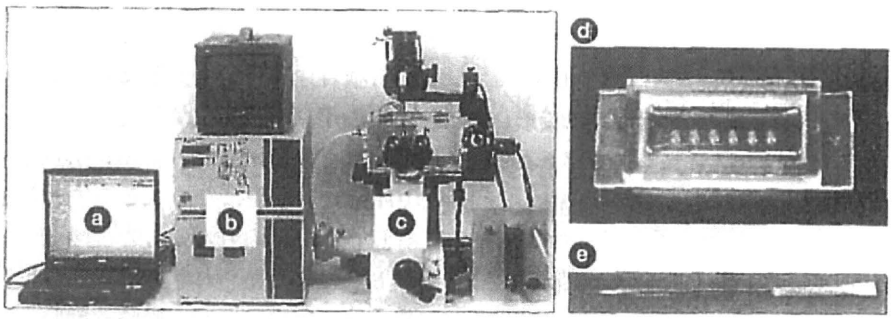

図1　受精卵呼吸測定装置（HV-403）
解析用PC（ⓐ），ポテンショスタット/コントローラ（ⓑ），倒立顕微鏡（ⓒ）で構成されている。倒立顕微鏡のステージ上に測定プレート(ⓓ)と微小白金電極(ⓔ)をセットして計測を行う。

表1　マウス胚移植試験の成績

実験区	受容雌（匹）	移植胚数（個）	移植胚の平均呼吸量（$\times10^{-14}$mol/s）	分娩した受容雌（匹）	分娩率（%）	産子数（匹）	産子率（%）
測定群（0.70以上）	16	170	0.85±0.01	12	12/16* (75.0)	67	67/170* (39.4)
対照群	18	175	—	7	7/18 (38.9)	41	41/175 (23.4)

*：対照区と比較して有意に高い（$p<0.05$）

I. 実　験

1. 材　料

C57BL/6マウスを実験に用いた。雌マウス（8週齢）にpregnant mare's serum gonadotropin（PMSG）5 IU投与し，48時間後にhuman chorionic gonadotropin（hCG）5 IU投与することで過排卵を誘発した。hCG投与後，直ちに同系統の雄マウスと同居させ，翌朝，腟栓の有無を確認した。腟栓を確認した雌マウスはhCG投与96時間後に屠殺し，摘出した子宮を灌流することで胚を回収した。卵割が停止しているなど明らかに異常が認められた胚を排除し，形態的に正常な胚盤胞のみを実験に使用した。

2. 呼吸活性測定

マウス胚盤胞の呼吸活性測定には，走査型電気化学顕微鏡を改良した受精卵呼吸測定装置（HV-403：図1，機能性ペプチド研究所）を用いた。呼吸測定液（ERAM-2：機能性ペプチド研究所）で満たした測定プレートの逆円錐形マイクロウェル内に胚を一つずつ静置した。その後，測定プレートを倒立顕微鏡のステージ上にセットし，−0.6 V vs $Ag/AgCl_2$の電位を印加した微小白金電極（先端直径：2〜3 μm）で，胚近傍を鉛直方向に4回走査(31.0 μm/sec, 160 μm)した。得られた胚近傍および沖合の酸素還元電流値の差から，球面拡散理論式[9]に基づいて胚の酸素消費量（呼吸活性）を算出した。

3. 胚移植試験

受精卵呼吸測定装置による胚品質評価の有効性を検証する目的で，胚移植試験を実施した（表1）。呼吸活性0.70×10^{-14}mol/s以上の胚盤胞を選別し，偽妊娠3日目の受容雌マウス（ICR）の子宮内に，1匹当たりの移植胚数が10個前後となるように移植した（測定群）。移植後17日目に分娩および産子数を確認した。呼吸測定を行

わずに形態観察により胚盤胞と判定した胚を移植した対照群では，18匹の受容雌マウスに合計175個の胚を移植した結果，7匹が分娩（38.9%）し，合計41匹の産子を得た（産子率：23.4%）。一方，測定群では16匹の受容雌マウスに合計170個の胚を移植した結果，12匹が分娩し（分娩率：75.0%），合計67匹の産子が得られ（産子率：39.4%），対照群と比較して移植成績が有意に上昇した。

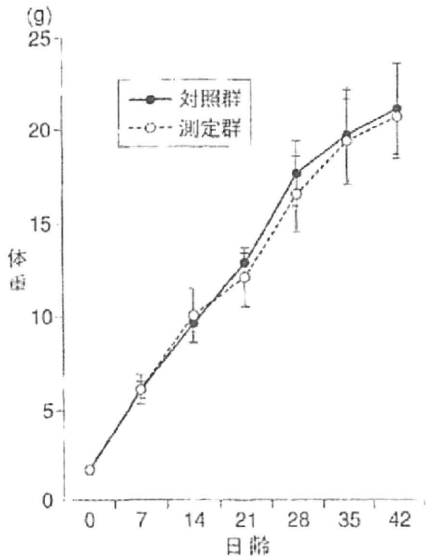

図2　体重成長曲線
生後0～42日の体重変化を示す。
（エラーバーは平均値±標準誤差）

4．表現型解析

受精卵呼吸測定装置による胚品質評価の安全性を検証する目的で，胚移植試験で得られた産子の表現型解析を実施した。産子の生時体重の平均は，対照群で1.55±0.02 g，測定群で1.51±0.04 gで有意差はなく，その後の体重増加にも有意差は認められなかった（図2）。また，Gバンド法による染色体検査（図3）や主要臓器（脳，肺，胃，腎臓，肝臓，膵臓，脾臓，心臓，大腿二頭筋，卵巣，精巣）の組織学的検査，血液生化学検査においても異常所見は認められなかった。また，行動解析（一般活動性・情動性・馴

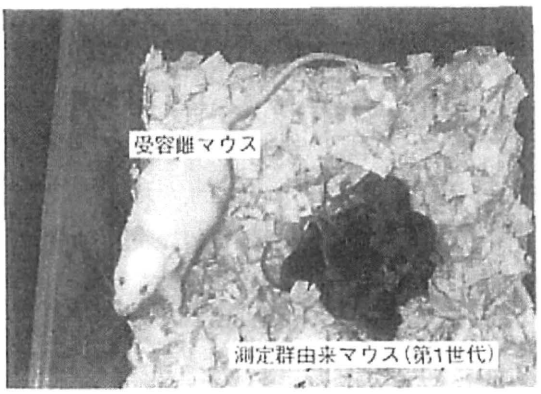

図4　測定群由来のマウス
性成熟後，5世代までの繁殖試験を実施したが，いずれの世代でも繁殖能力に異常はみられなかった。

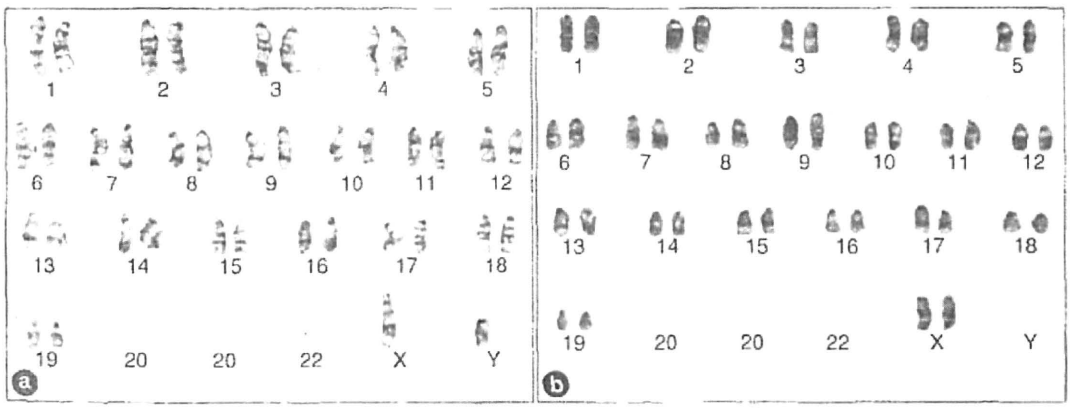

【雄マウス】　【雌マウス】

図3　染色体解析（Gバンド解析）
解析したマウス（30匹：雄12匹，雌18匹）すべてが2n＝40の正常な核型を有していた。

化の試験としてオープンフィールドテスト，運動能力・体力の試験としてオープンスペース水泳テスト，空間認知・学習能力・記憶力の試験として水迷路学習テストおよびプローブテスト）を実施したが，いずれのテストにおいても対照群と測定群のマウスで有意差は認められなかった。さらに，測定群の産子は性成熟後に繁殖試験を実施し，少なくとも5世代目までは正常な繁殖能力を有していることが確認された(図4)。

II. 考　察

近年の不妊治療件数の増加とともに多胎妊娠数も増加している。わが国では，生殖補助医療に伴って発生する多胎妊娠を減少させることが急務であるとし，2007年3月には日本生殖医学会が「多胎妊娠防止のための移植胚数ガイドライン」を，2008年4月には日本産科婦人科学会が「生殖補助医療における多胎妊娠防止に関する見解」を発表している。いずれの内容も，母体および胎児・新生児の健全なる福祉を保持する観点から，35歳以下の患者に対する胚移植においては，移植する胚の数を「原則1個」とすることが示されている。また，Veleva ら[5]は，36～39歳の患者に対しても単一胚移植を実施し，妊娠率，正常分娩率が複数胚（2個）移植の場合と比較して統計的有意差がないことを報告している。これらのことから，生殖補助医療における単一胚移植は，今後，幅広い年齢層の患者に対してますます重要になってくる可能性が考えられる。

単一胚移植における胚の評価に求められることは，できるだけ低侵襲に，再現性の高い方法で，移植に供する個々の胚の品質を正確に評価・選別することである。このことは妊娠率の向上だけではなく，流産・死産率の低下にもつながる。現在，生殖補助医療の臨床現場の多くは，Veeck[6]や Gardner ら[7]が提唱したヒト胚の品質評価法を採用している。これらの評価方法は，胚の割球数や形態を基準としており，現状では，最も簡便で有効な方法である。しかしながら，最近，経時的な胚の観察研究などから，胚の品質を評価する上で形態を基準にするだけでは決して十分ではないことが指摘されている[8][9]。また，形態的基準による判断だけでは，観察者の主観が影響する可能性が高く，検査結果の客観性に疑問が残る。

一方で，本研究で使用した受精卵呼吸測定装置は，個々の胚の酸素消費量を数値化できるため，客観的に胚の評価・選別が可能である。本研究では，妊娠4日目のマウスから得られた胚盤胞を①形態的基準のみで評価した胚（対照群）と②形態評価に加え呼吸活性を評価基準に評価した胚（測定群）に分けて移植した結果，測定群は対照群と比較して妊娠率，産子率が有意に上昇することが確認された。同様の結果は，ウシを用いた胚移植試験においても得られている[9][10]。さらに本研究では，得られた産子の正常性についても様々な角度から検証し，呼吸活性を測定した胚を移植しても，その産子に異常はみられないことを確認した。従って，これらの結果から，胚の評価に呼吸活性の指標を加えることは，従来の形態的基準のみで評価する方法よりも有効な方法であり，胚やその後の個体発生への影響が少ない安全な方法であることが示唆された。

今回の結果はマウス胚を用いたものであり，ヒト胚における有効性，安全性については今後の課題である。しかしながら，この測定技術の注目すべき点は胚の酸素消費量（ミトコンドリア機能）を評価していることである。ミトコンドリアはすべての真核細胞に普遍的に存在している細胞内小器官である。従って，本研究で得られたマウスの結果をヒトへ直接外挿できる可能性は高いとわれわれは考えている。

おわりに

本研究では，マウスをモデル動物として，受精卵呼吸測定装置の有効性と安全性を検証した。その結果，呼吸活性を指標として胚の品質

を評価することで，移植成績の向上が認められた。さらに，得られた産子に異常所見はみられなかった。これらの結果から，電気化学的な胚の呼吸測定技術が，胚移植時における胚の品質評価法として有効かつ安全であることが示唆された。今後，ヒト胚における検証を十分に重ねるとともに，胚の呼吸活性と受胎（妊娠）との関係を詳しく調べることで，さらに安全性や精度を高めることができると考えている。近い将来，呼吸測定技術および装置が生殖補助医療における臨床応用へつながっていくことを期待している。

文　献

1) Shiku H, Shiraishi T, Ohya H, et al : Oxygen consumption of single bovine embryos probed by scanning electrochemical microscopy. Anal Chem, 73 : 3751-3758, 2001.
2) Shiku H, Shiraishi T, Aoyagi S, et al : Respiration activity of single bovine embryos entrapped in a cone-shaped microwell monitored by scanning electrochemical microscopy. Anal Chim Acta, 522 : 51-58, 2004.
3) Abe H, Shiku H, Yokoo M, et al : Evaluating the quality of individual embryos with a non-invasive and highly sensitive measurement of oxygen consumption by scanning electrochemical microscopy. J Reprod Dev, 52(supple): s55-s64, 2006.
4) Abe H : A non-invasive and sensitive method for measuring cellular respiration with a scanning electrochemical microscopy to evaluate embryo quality. J Mamm Ova Res, 24 : 70-78, 2007.
5) Veleva Z, Vilska S, Hydén-Granskog C, et al : Elective single embryo transfer in women aged 36-39 years. Hum Reprod, 21 : 2098-2102, 2006.
6) Veeck LL : Atlas of the human oocytes and early conceptus, Williams & Wilkins, 2, 151-153, Baltimore, 1991.
7) Gardner DK, Lane M, Stevens J, et al : Blastocyst score affects implantation and pregnancy outcome : towards a single blastocyst transfer. Fertil Steril, 73 : 1155-1158, 2000.
8) Mio Y, Maeda K : Time-lapse cinematography of dynamic changes occurring during *in vitro* development of human embryos. Am J Obstet Gynecol, 660 : e1-5, 2008.
9) Okitsu O : Human embryo grading. J Mamm Ova Res, 25 : 90-97, 2008.
10) Moriyasu S, Hirayama H, Sawai K, et al : Relationship between the respiratory activity and the pregnancy rate of bisected bovine. Reprod Fertil Dev, 19 : 219, 2007.

胚の機能検定法

阿部宏之

ミトコンドリアは酸素呼吸によって細胞活動に必須のエネルギーを合成する重要な細胞小器官であり，その呼吸機能は胚や卵子の代謝活性解析やクオリティ評価の有力な指標となる．したがって，精度の高い細胞呼吸計測法は，胚の厳密なクオリティ評価や細胞機能解析にきわめて重要な技術となる．

本稿では，高精度・非侵襲的に細胞呼吸を測定することができる電気化学計測技術を応用した“受精卵呼吸測定装置”と，この装置を用いた胚の呼吸機能解析とクオリティ評価法について述べる．

電気化学計測法と受精卵呼吸測定装置

電気化学計測法は，プローブ電極による酸化還元反応を利用し，局所領域における生物反応を電気化学的に高精度で検出できる有効な技術である．酸素の還元電位を検出するマイクロ電極をプローブとする走査型電気化学顕微鏡(SECM)を用いることで，細胞が消費する酸素量を無侵襲的に測定することができる．

このSECMをベースに胚の呼吸量測定のためのシステムとして，“受精卵呼吸測定装置”が開発されている[1]．この測定システムは，倒立型顕微鏡(図1①)，マイクロ電極の電位を一定に保持するポテンショスタット(図1②)，マイクロ電極の移動を制御するコントローラー(図1③)，短時間で酸素消費量を算出する専用の解析ソフトを内蔵したノート型コンピュータ(図1④)により構成されている．倒立型顕微鏡のステージ上には，保温プレート，マイクロ電極の三次元走査を可能とするXYZステージが設置されており，気相条件を制御するための測定用チャンバーの設置も可能である．

胚の呼吸量測定

受精卵呼吸測定装置を用いた呼吸量測定には，超高感度のディスク型マイクロ電極(図2a)，専用の多検体測定プレートと測定液を用いる．多検体測定プレートは測定操作の簡易化を目的に開発され，プレートの底面には円錐形のマイクロウェル6穴が施されている(図2b)．マイクロ電極が検出する微弱な電流値は溶液の成分によって値が変動するため，呼吸測定には胚および細胞用培養液をベースに調製した専用の測定液を用いる．

測定液を満たしたマイクロウェル内に胚を導入した後，ウェルの底部中心に静置する(図2c)．胚の半径値を解析ソフトに入力した後，マイクロ電極を胚の透明帯直近に手動で移動させる．マイクロ電極は，酸素が還元可能な−0.6 V vs. Ag/AgClに電位を保持した後，コンピュータ制御により透明帯近傍を鉛直(Z軸)方向に走査する(図2d)．通常，1試料当たりマイクロ電極を2〜3回走査し，呼吸量を測定する(所要時間は約30秒)．マイクロ電極走査後，胚の酸素消費量は球面拡散理論式[2]を基盤とする呼吸解析ソフトを用いて算出する(図3)．波形の始点(マイクロ電極が胚に最も接近している)と終点(マイクロ電極が胚から最も離れている)の電流値の差(ΔC)から呼吸量を算出する(ΔC

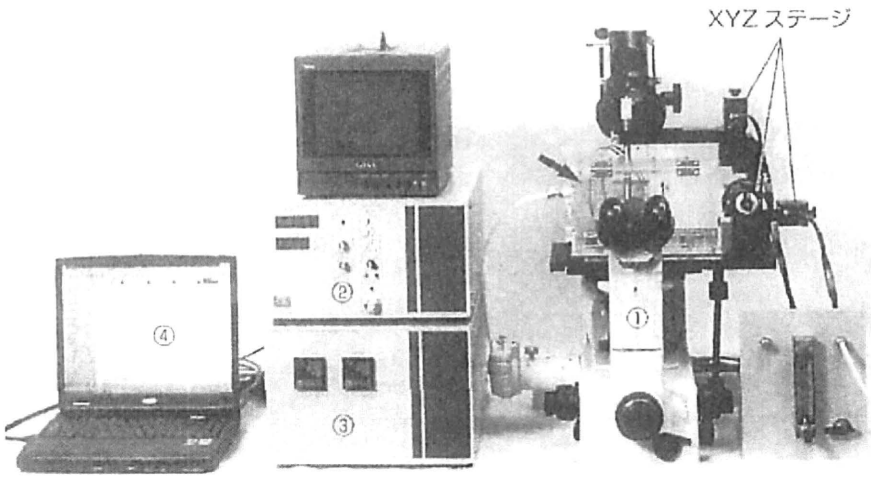

図1　走査型電気化学顕微鏡をベースに開発した受精卵呼吸測定装置
①：倒立型顕微鏡（矢印は測定チャンバーを示す），②：ポテンショスタット，③：コントローラー，④ノートパソコン（呼吸機能解析ソフトを内蔵）．

が大きいほど胚の呼吸量は大きい）．

胚のミトコンドリア呼吸機能

受精卵呼吸測定装置を用いて，種々の哺乳動物胚の呼吸量を測定することができる．

図4に，マウス胚の発生過程における呼吸量変化を示す．マウス胚の呼吸量は，受精直後の1細胞期から8細胞期までは0.5×10^{-17} mol・sec^{-1}前後と低い．桑実胚から胚盤胞にかけて呼吸量は増加し，発生が進み細胞数も増加した孵化胚盤胞では最も高い呼吸活性が計測される．

ミトコンドリアは呼吸機能の成熟に伴い顕著な微細構造変化を起こすことから，電子顕微鏡による胚の微細構造観察は呼吸測定の有効性を検証するために重要である．マウス胚の微細構造を観察すると，呼吸活性の低い2細胞期胚ではミトコンドリアのほとんどは未成熟であるが，呼吸量が増加する胚盤胞ではミトコンドリアの顕著な発達（クリステの拡張）が起こる（図5）．

このように，ミトコンドリアの発達と呼吸量の増加は一致することから，受精卵呼吸測定装置による呼吸測定は，胚のミトコンドリア呼吸機能解析に有効な方法であることがわかる．

呼吸機能解析と胚のクオリティ評価

体外受精・胚移植（*in vitro* fertilization and embryo transfer：IVF-ET）は，最も有効な不妊治療法の一つである．一般にIVF-ETでは，IVFによって得られた複数の胚のなかから移植する胚を選択する．胚移植前に質的に最も良好な胚を選択することは，妊娠率の向上，多胎妊娠の回避，流産率の低下のために有効である．

現在，胚のクオリティ評価は形態観察による方法が一般的である．形態的評価法は，簡単・迅速で無侵襲的な方法であることから，現状では最も有効な胚のクオリティ評価法であると言える．しかし，評価の基準となる形態的特徴は定量性に欠けるため，判定結果が観察者の主観に左右される可能性がある．これまでの研究によって，ミトコンドリア呼吸機能と胚のクオリティは深く関係することが明らかになっており，受精卵呼吸測定装置による呼吸量測定は胚クオリティ評価の有力な指標になると考えられる．

ウシにおいて，胚のクオリティと呼吸活性の

283-01343

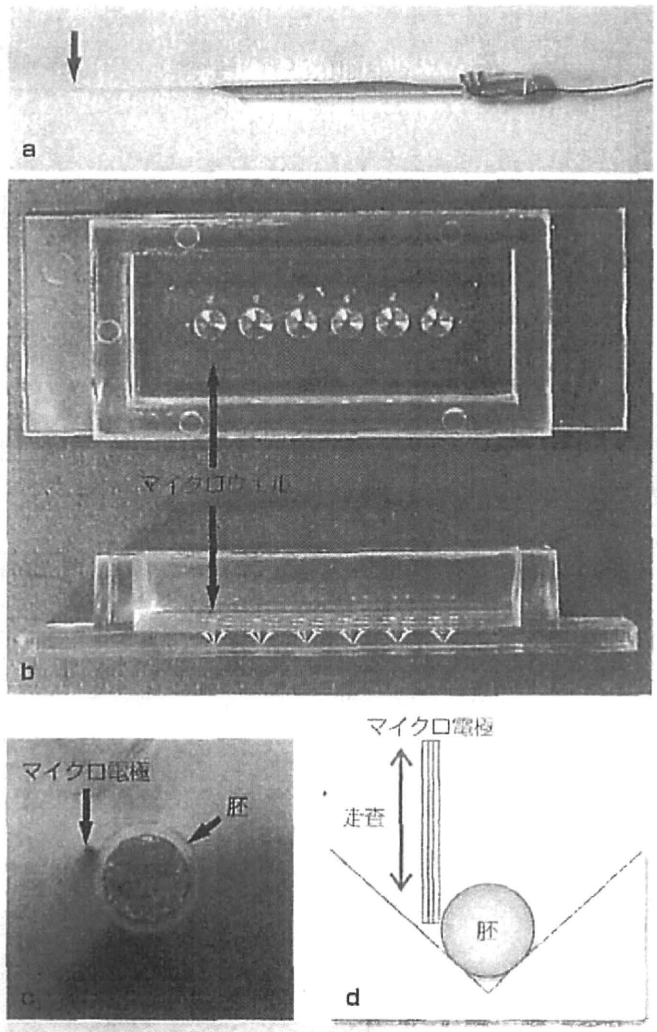

図2　胚の呼吸測定のための関連技術
a：ディスク型白金マイクロ電極.
b：多検体測定プレート．底面には円錐形のマイクロウェルが6穴施されている.
c：マイクロウェル底部に静置したウシ胚.
d：マイクロ電極は胚近傍を鉛直方向に走査し，胚の酸素消費量を測定する.

関係を示す興味深い研究成果が得られている．呼吸測定後の胚を借腹牛に移植し胚の呼吸活性と受胎率の関係を調べた結果，移植前の呼吸量が基準値以上(胚盤胞で 1.0×10^{14}/mol・sec^{-1}，初期胚盤胞で 0.8×10^{14}/mol・sec^{-1}，桑実胚で 0.5×10^{14}/mol・sec^{-1}) の胚を移植した場合，60%以上の高い妊娠率が得られている．一方，呼吸量が基準値以下の胚は，ほとんど受胎しない．この研究結果から，受精卵呼吸測定装置はクオリティ良好胚の選別に有効なシステムであると考えられている[3]．

ヒト胚の呼吸機能解析

受精卵呼吸測定装置は，ほとんどの細胞に共通するミトコンドリア呼吸を測定していることから汎用性は高く，ヒト胚の呼吸機能解析やクオリティ評価への応用が期待されている．

ヒトへの応用を目的とした基礎的研究として，ヒト胚（余剰胚）の形態と呼吸測定例を示す(図6)．体外受精3日(day 3)および5日(day 5)の胚の酸素消費量は，それぞれ 0.45×10^{14}/mol・sec^{-1} および 1.15×10^{14}/mol・sec^{-1} で

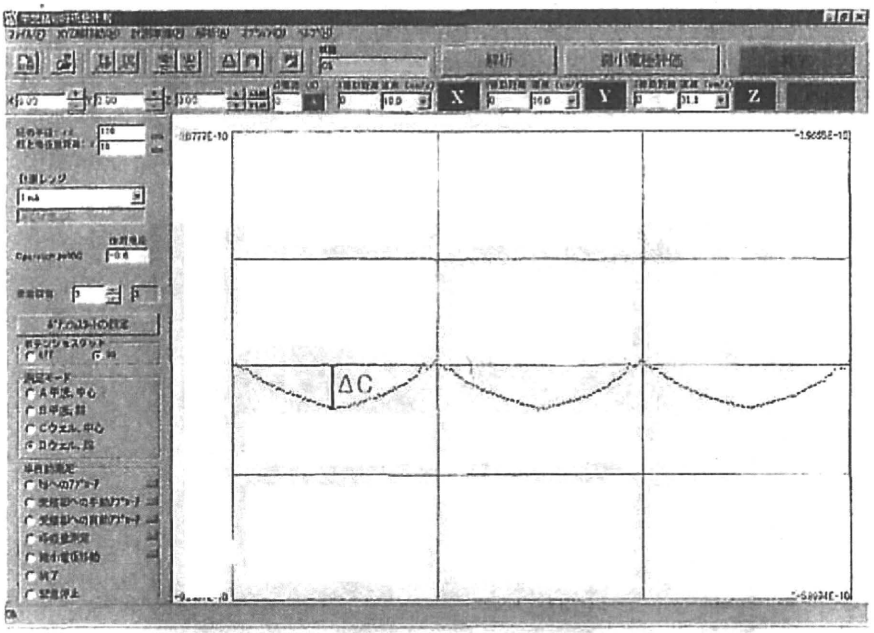

図3　呼吸解析ソフトの画面
マイクロ電極の走査の始点と終点の電流値の差（ΔC）から胚の酸素消費量（呼吸）を算出する．

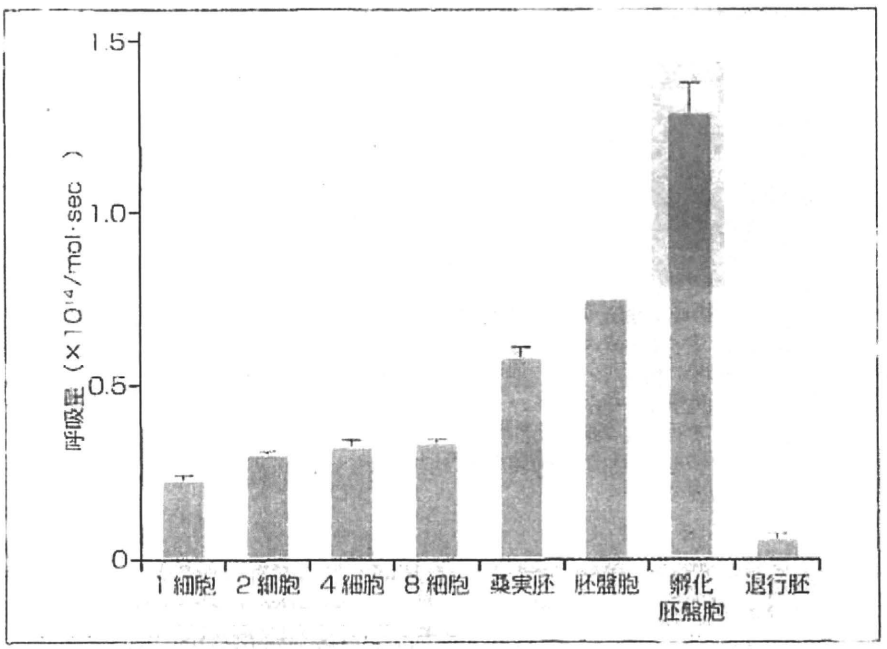

図4　マウス胚の発生過程における呼吸量変化
桑実胚から胚盤胞期にかけて呼吸量が増加する．

あり，発生が進んだ胚の呼吸活性は高い傾向にある．電子顕微鏡を用いたミトコンドリアの微細構造解析により，day 5胚では発達したミトコンドリアが多く観察される．このようにヒト胚においても，受精卵呼吸測定装置を用いたミトコンドリア呼吸機能解析研究が進んでいる．

今後，IVF-ETを中心とする不妊治療成績の向上には，移植の対象となる胚のクオリティ評価がこれまで以上に重要になってくる．精度の高い胚クオリティ評価法確立のためには，現行の形態的評価法と比べて客観性の高いクオリティ評価法の開発が不可欠である．

263-01343

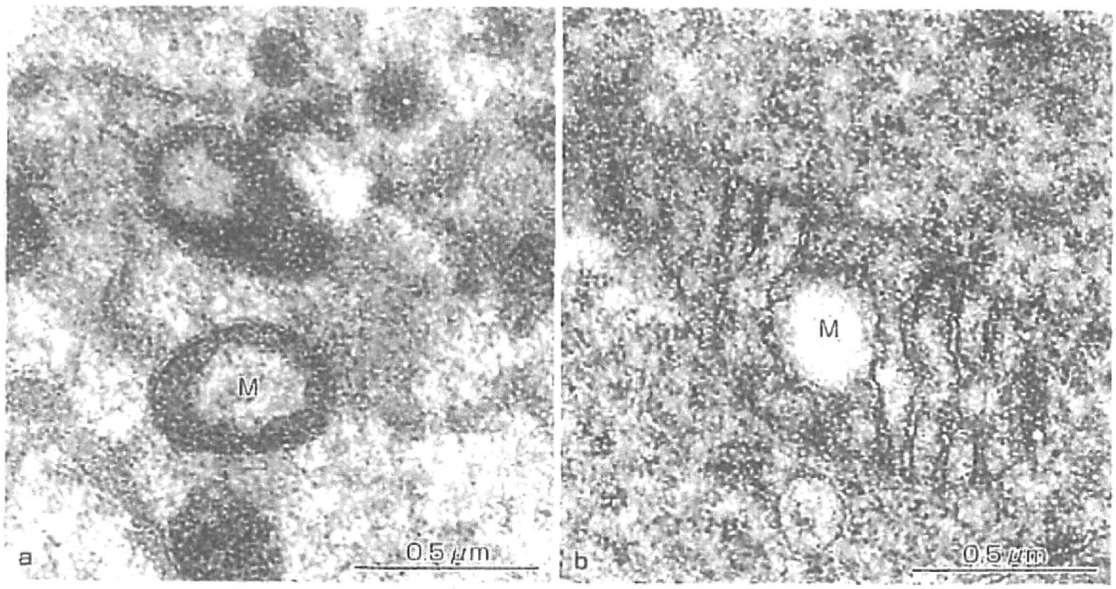

図5　マウス胚のミトコンドリアの微細形態
a：2細胞期胚，b：胚盤胞．M：ミトコンドリア．

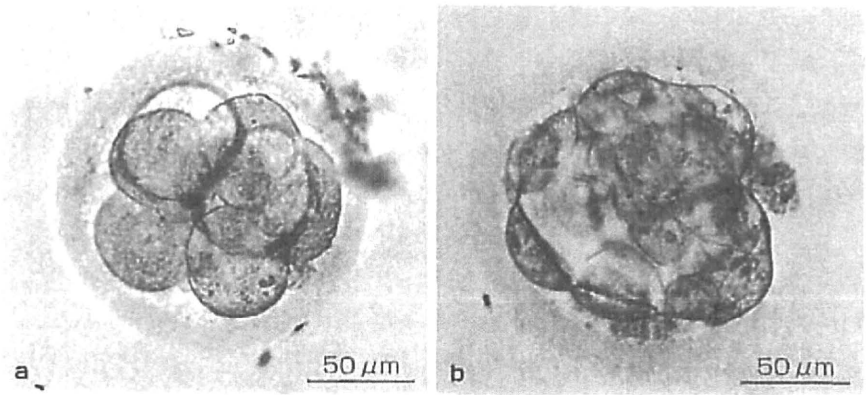

図6　ヒト体外受精胚の形態と酸素消費量
a：day 3 胚 (0.45×10^{-14}/mol・sec^{-1})，b：胚盤胞 (1.15×10^{-14}/mol・sec^{-1})．

本稿で述べた受精卵呼吸測定装置は，高精度・非侵襲的に胚の呼吸代謝機能を解析できることから，新しい胚のクオリティ評価の有効な基盤技術として期待できる．

文献

1) Abe H, Shiku H, Aoyagi S, et al. In vitro culture and evaluation of embryos for production of high quality bovine embryos. J Mamm Ova Res. 2004; 21: 22-30.
2) Shiku H, Shiraishi T, Ohya H, et al. Oxygen consumption of single bovine embryos probed with scanning electrochemical microscopy. Anal Chem. 2001; 73: 3751-8.
3) Abe H, Shiku H, Yokoo M, et al. Evaluating the quality of individual embryos with a non-invasive and highly sensitive measurement of oxygen consumption by scanning electrochemical microscopy. J Reprod Dev. 2006; 52 (Suppl): S55-61.

263-01343

Uterine FK506-binding protein 52 (FKBP52)–peroxiredoxin-6 (PRDX6) signaling protects pregnancy from overt oxidative stress

Yasushi Hirota[a,b,1], Nuray Acar[a,c,1], Susanne Tranguch[a], Kristin E. Burnum[d], Huirong Xie[a], Ako Kodama[b], Yutaka Osuga[b], Ismail Ustunel[c], David B. Friedman[d], Richard M. Caprioli[d], Takiko Daikoku[a], and Sudhansu K. Dey[a,2]

[a]Division of Reproductive Sciences, The Perinatal Institute, Cincinnati Children's Hospital Medical Center, University of Cincinnati College of Medicine, Cincinnati, OH 45229; [b]Department of Obstetrics and Gynecology, University of Tokyo, Tokyo 113-8655, Japan; [c]Department of Histology and Embryology, School of Medicine, Akdeniz University, Antalya 07070, Turkey; and [d]Mass Spectrometry Research Center, Vanderbilt University Medical Center, Nashville, TN 37232

Edited by Bert W. O'Malley, Baylor College of Medicine, Houston, TX, and approved July 26, 2010 (received for review July 1, 2010)

Immunophilin FK506-binding protein 52 (FKBP52) is a cochaperone that binds to the progesterone receptor (PR) to optimize progesterone (P_4)-PR signaling. We recently showed that *Fkbp52*-deficient (*Fkbp52*$^{-/-}$) mice have reduced uterine PR responsiveness and implantation failure which is rescued by excess P_4 supplementation in a genetic background-dependent manner. This finding led us to hypothesize that FKBP52 has functions in addition to optimizing PR activity. Using proteomics analysis, we found that uterine levels of peroxiredoxin-6 (PRDX6), a unique antioxidant, are significantly lower in *Fkbp52*$^{-/-}$ mice than in WT and PR-null (*Pgr*$^{-/-}$) mice. We also found that *Fkbp52*$^{-/-}$ mice with reduced uterine PRDX6 levels are susceptible to paraquat-induced oxidative stress (OS), leading to implantation failure even with P_4 supplementation. The same dose of paraquat did not interfere with implantation in WT mice. Moreover, treatment with antioxidants α-tocopherol and N-acetylcysteine (NAC) attenuated paraquat-induced implantation failure in P_4-treated *Fkbp52*$^{-/-}$ mice. Functional analyses using mouse embryonic fibroblasts show that *Fkbp52* deficiency associated with reduced PRDX6 levels promotes H_2O_2-induced cell death, which is reversed by the addition of NAC or by forced expression of PRDX6, suggesting that *Fkbp52* deficiency diminishes the threshold against OS by reducing PRDX6 levels. These findings provide evidence that heightened uterine OS in *Fkbp52*$^{-/-}$ females with reduced PRDX6 levels induces implantation failure even in the presence of excess P_4. This study shows that FKBP52–PRDX6 signaling protects pregnancy from overt OS.

embryo implantation | mouse | uterus

Infertility is a global social and economic concern. It is estimated that by 2050 15% of couples worldwide will be childless because of infertility. Although many causes of infertility have been overcome by the application of in vitro fertilization and embryo transfer (IVF-ET), implantation failure is still a major obstacle for optimal pregnancy outcome. Pregnancy rates remain low in patients undergoing IVF-ET because of the transfer of embryos into a nonreceptive uterus, resulting in implantation failure (1). Heterogeneous uterine cell types respond differentially to estrogen and progesterone (P_4) to prepare the uterus to the receptive state. For successful implantation to occur, the uterus must be transiently receptive to implantation-competent blastocysts. P_4 signaling is an absolute requirement for implantation and pregnancy maintenance in most mammals studied (2). P_4 acts via the nuclear progesterone receptor (PR) to activate transcription of genes involved in ovulation, uterine receptivity, implantation, decidualization, and pregnancy maintenance (3).

We recently found that the immunophilin FK506-binding protein 52 (FKBP52) serves as a cochaperone to govern normal PR function in the mouse uterus, where its expression overlaps with that of PR. Immunophilins are so named because they bind to certain immunosuppressive drugs to mediate their actions. They are grouped into two families, FKBP and cyclosporin A-binding (cyclophilin, CyP) proteins. Some FKBP and CyP family members have a tetratricopeptide repeat (TPR) domain that targets binding to the conserved C terminus of Hsp90. FKBP52 is one such TPR-containing cochaperone that influences steroid hormone receptor function (4). The mature PR complex bound to FKBP52 binds to P_4 with high affinity and efficiency, although some basal PR responsiveness to P_4 is retained in the absence of FKBP52. In addition, FKBP52 plays a role in immunoregulation and basic cellular processes involving protein stability, folding, and trafficking (5–7).

We found that *Fkbp52*$^{-/-}$ females on both C57BL6/129 mixed and CD1 backgrounds have implantation failure with normal ovulation (8, 9). However, P_4 supplementation rescues implantation and decidualization in CD1, but not in C57BL6/129, *Fkbp52*$^{-/-}$ females. In CD1 *Fkbp52*$^{-/-}$ females, P_4 at higher-than-normal levels confers PR signaling sufficient for implantation, but even higher levels of P_4 are required to rescue full-term pregnancy (9). How P_4 overcomes reduced PR responsiveness to allow implantation in CD1 *Fkbp52*$^{-/-}$ mice is still unknown. Because FKBP52 positions PR in optimal conformation for binding to P_4, one possibility is that excess P_4 in the absence of FKBP52 increases the probability of random binding of P_4 to the PR complex even in its less optimal configuration. Alternatively, FKBP52 may influence other pathways along with PR signaling, because exogenous P_4 cannot rescue implantation in C57BL6/129 *Fkbp52*$^{-/-}$ mice and significantly higher P_4 levels are necessary to restore implantation and full-term pregnancy in CD1 *Fkbp52*$^{-/-}$ females (9). Moreover, *Fkbp52* also is expressed in the placenta with no detectable PR expression (9), implying that FKBP52 has other functions in addition to its role in optimizing PR activity. Our present study, using proteomics analysis, found that FKBP52 regulates oxidative stress (OS) by regulating the levels of a unique antioxidant, peroxiredoxin-6 (PRDX6), which operates independently of other peroxiredoxins and antioxidant proteins (10–12). Here we show that uterine FKBP52–PRDX6 signaling is a major player in countering the adverse effects of OS during early pregnancy.

Results

PRDX6 Levels Are Reduced in *Fkbp52*$^{-/-}$ Uteri. To explore downstream targets of FKBP52 independent of PR, we used proteomics approaches. Ovariectomized WT, *Fkbp52*$^{-/-}$, and PR-null (*Pgr*$^{-/-}$) mice on the C57BL6/129 background were treated with P_4 (2 mg/d) for 2 d, and uteri were collected 24 h after the second injection. Uterine protein lysates were subjected to 2D difference in gel electrophoresis (2D-DIGE) analysis with detection limits from 10- to 150-kDa proteins (pH 4–7) (Fig. 1*A*). Among the differentially expressed proteins, we found that PRDX6 levels are markedly down-regulated in *Fkbp52*$^{-/-}$ uteri compared with

Author contributions: Y.H., S.T., T.D., and S.K.D. designed research; Y.H., N.A., S.T., K.E.B., H.X., A.K., Y.O., D.B.F., and T.D. performed research; R.M.C. contributed new reagents/analytic tools; Y.H., N.A., S.T., I.U., T.D., and S.K.D. analyzed data; and Y.H., S.T., T.D., and S.K.D. wrote the paper.

The authors declare no conflict of interest.

This article is a PNAS Direct Submission.

[1]Y.H. and N.A. contributed equally to this work.

[2]To whom correspondence should be addressed. E-mail: sk.dey@cchmc.org.

This article contains supporting information online at www.pnas.org/lookup/suppl/doi:10.1073/pnas.1009324107/-/DCSupplemental.

$Pgr^{-/-}$ and WT uteri, with the exception of FKBP52, serving as an internal control (Table S1 and Fig. 1*B*). This finding led us to focus on PRDX6 as a potential downstream mediator of FKBP52 function, independent of its PR cochaperone activity, and to assess uterine expression of *Prdx6* in early pregnancy. Notably, we found that levels of six proteins increased in $Fkbp52^{-/-}$ uteri compared with WT uteri, but no differences were detected between WT and $Pgr^{-/-}$ uteri (Table S2). We confirmed down-regulated PRDX6 protein levels in $Fkbp52^{-/-}$ uteri compared with $Pgr^{-/-}$ and WT uteri by Western blotting (Fig. 1 *C* and *D*) and immunohistochemistry (Fig. 1*E*). In addition, both stromal and epithelial localization of PRDX6 was reduced in ovariectomized $Fkbp52^{-/-}$ uteri treated with P_4 (Fig. 1*E*).

To examine the effects of ovarian hormones on *Prdx6* expression in mouse uteri, we performed Northern and in situ hybridization using uteri from ovariectomized WT mice. Neither P_4 nor estradiol-17β (E_2) significantly altered *Prdx6* expression levels (Fig. S1*A*), but P_4 changed the expression domain from the epithelium to the stroma (Fig. S1*B*).

PRDX6 Is Aberrantly Expressed in $Fkbp52^{-/-}$ Uteri. On day 4 of pregnancy the uterus is under the influence of P_4 produced by the newly formed corpus luteum. PRDX6 is localized in both the stroma and epithelium in WT CD1 mice on day 4 of pregnancy (Fig. 1*F*). In contrast, in $Fkbp52^{-/-}$ uteri PRDX6 is restricted primarily to the epithelium but is localized in the subluminal stroma after P_4 supplementation (Fig. 1*F*). These results suggest that FKBP52 deficiency attenuates PRDX6 levels in the stroma that are compensated to some extent by P_4.

PRDX6 Is Differentially Expressed in Uteri During Early Pregnancy. The uterus is under the influence of preovulatory estrogen with increased epithelial cell proliferation on day 1 of pregnancy. On day 4, the uterus is exposed to heightened P_4 levels along with a small amount of estrogen, resulting in epithelial cell differentiation with stromal cell proliferation. The first molecular and physical interaction between the blastocyst and receptive uterus is observed on the evening of day 4, and the attachment process continues through day 5. The attachment reaction coincides with increased stromal vascular permeability solely at the site of the blastocyst and can be demarcated by distinct blue bands along the uterus after i.v. injection of a blue dye solution (13). The proliferating stromal cells surrounding the implanting blastocyst start to differentiate to decidual cells in the afternoon of day 5. Differentiating stromal cells in the immediate vicinity of the implanting blastocyst begin to form the primary decidual zone (PDZ) at this time. The PDZ is well formed on day 6 with the beginning of a proliferating secondary decidual zone (SDZ). Although cell proliferation ceases in the PDZ, it continues in the SDZ. The PDZ progressively degenerates as pregnancy progresses. On day 8, the implantation process is well advanced with maximal decidualization. We assessed *Prdx6* expression on days 1, 4, 5, and 8 of pregnancy by in situ hybridization. We found that *Prdx6* is detected mostly in the luminal epithelium on day 1 (Fig. 2*A*). On day 4, the expression is restricted to the stroma (Fig. 2*A*). *Prdx6* expression on these days closely resembles that of *Fkbp52* (14). On day 5, *Fkbp52* and *Prdx6* are expressed in a similar fashion in the decidualizing stroma surrounding the implanting blastocyst (Fig. 2 *A* and *B*). This overlapping expression of *Fkbp52* and *Prdx6* surrounding the implanting blastocyst suggests that the process of implantation may regulate these two molecules. On day 8, *Prdx6* is expressed primarily in the SDZ cells and in the embryo. PRDX6 protein levels also are up-regulated in uteri on days 5 and 8 of pregnancy (Fig. 2 *C* and *D*). In the placenta, *Fkbp52* and *Prdx6* showed a similar expression pattern in the labyrinth layer (Fig. 2*B*), with undetectable levels of PR (9). The similar localization of FKBP52 and PRDX6 in the deciduum and placenta suggests their PR-independent roles in these tissues. Furthermore, pull-down assays show that FKBP52 is physically

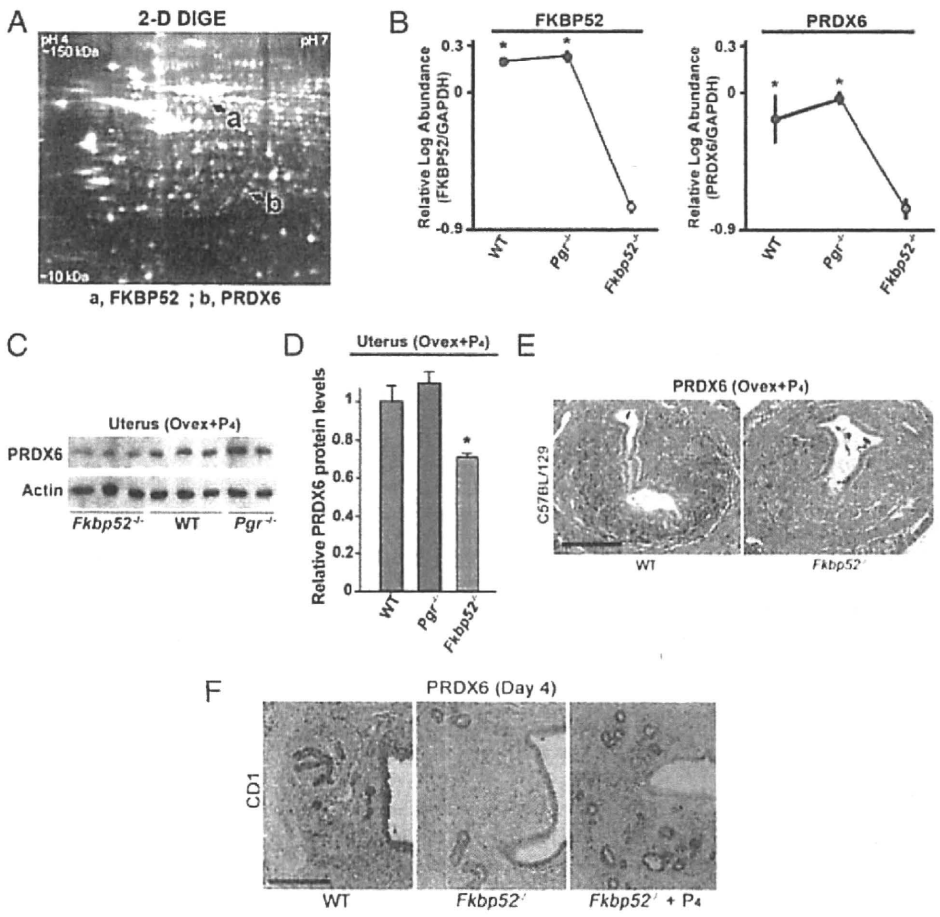

Fig. 1. PRDX6 expression is reduced in uteri of $Fkbp52^{-/-}$ mice. (*A*) A representative DIGE gel comprising protein extracts from WT and $Fkbp52^{-/-}$ uteri shows proteins of isoelectric points between pH 4–7 and apparent molecular mass between 10–150 kDa. a, FKBP52; b, PRDX6. (*B*) Decreased protein levels of PRDX6 and FKBP52 in P_4-treated uteri of $Fkbp52^{-/-}$ ovariectomized mice ($n = 4$) compared with WT ($n = 3$) and $Pgr^{-/-}$ ($n = 3$) ovariectomized mice on a C57BL6/129 background. Values are mean ± SEM. $^*P < 0.05$ compared with $Fkbp52^{-/-}$ mice. (*C* and *D*) Decreased PRDX6 protein levels in P_4-treated uteri of $Fkbp52^{-/-}$ ovariectomized mice compared with WT and $Pgr^{-/-}$ ovariectomized females as determined by Western blotting. Band intensities are normalized against actin and expressed as relative ratios compared with WT samples on the C57BL6/129 background. Values are mean ± SEM of two or three independent samples. $^*P < 0.05$ compared with WT mice. (*E*) Differential expression patterns of PRDX6 protein in P_4-treated ovariectomized mouse uteri of WT and $Fkbp52^{-/-}$ mice on the C57BL6/129 background. (Scale bar, 200 μm.) (*F*) Differential expression patterns of PRDX6 protein in day 4 uteri of WT and $Fkbp52^{-/-}$ mice on a CD1 background. (Scale bar, 200 μm.)

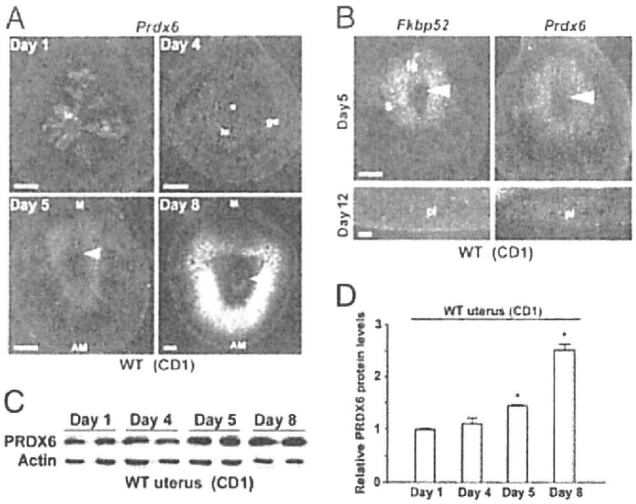

Fig. 2. Uterine PRDX6 is expressed differentially during early pregnancy. (*A*) In situ hybridization showing spatiotemporal expression of *Prdx6* in WT CD1 uteri on days 1, 4, 5, and 8 of pregnancy. Arrowheads indicate implanting embryos. AM, antimesometrial pole; ge, glandular epithelium; le, luminal epithelium; M, mesometrial pole; s, stroma. (Scale bar, 200 μm.) (*B*) Overlapping expression of *Fkbp52* and *Prdx6* in CD1 WT uteri on days 5 and 12 of pregnancy. Arrowheads indicate implanting embryos. le, luminal epithelium; pl, placenta; s, stroma. (Scale bars, 200 μm.) (*C* and *D*) Levels of uterine PRDX6 protein during early pregnancy as determined by Western blotting. Band intensities of PRDX6 were normalized against actin. Two independent samples from different mice were examined in each group. Data are expressed as mean ± SEM. $^*P < 0.05$ compared with day 1 uteri.

associated with PRDX6 in the deciduum (Fig. S2), suggesting that FKBP52 influences PRDX6 status through this interaction.

In the human endometrium, both PRDX6 and FKBP52 are expressed in epithelial cells during the proliferative phase and in both epithelial and stromal cells in the secretory phase (Fig. S3*A*). The higher levels of *Prdx6* in the secretory (receptive) phase suggest that uterine PRDX6 also plays antioxidant roles in human implantation (Fig. S3*B*).

***Fkbp52*$^{-/-}$ Uteri Are More Prone to Overt OS During Implantation.** Because PRDX6 levels are reduced in *Fkbp52*$^{-/-}$ uteri on day 4 of pregnancy, especially in the stroma (Fig. 1*F*), we speculated that *Fkbp52*$^{-/-}$ uteri are more susceptible to OS during implantation. We have shown previously that P_4 levels are comparable in WT and *Fkbp52*$^{-/-}$ mice. However, excess P_4 supplementation that markedly elevates circulating P_4 levels is required for implantation in *Fkbp52*$^{-/-}$ females (9). Although P_4 supplementation rescues implantation failure in CD1 *Fkbp52*$^{-/-}$ mice (9), concomitant administration of the OS-inducing agent paraquat (15 or 20 mg/kg) prevented this rescue (Table 1 and Fig. 3*A*). In contrast, similar doses of paraquat failed to affect implantation in WT mice (Table 1 and Fig. 3*A*). To minimize the detrimental effects of paraquat on embryo growth and activation, we also performed embryo-transfer experiments. Day 4 WT blastocysts were transferred into day 4 WT or P_4-treated *Fkbp52*$^{-/-}$ recipients that received paraquat 7 h before the embryo transfer. Again, *Fkbp52*$^{-/-}$ mice had reduced numbers of implantation sites, whereas WT recipients showed normal implantation when examined on day 5 (Table 2). It is interesting that even a smaller dose of paraquat (2 mg/kg) inhibited implantation in P_4-treated *Fkbp52*$^{-/-}$ mice (Table 3). These results suggest that *Fkbp52*$^{-/-}$ mice are quite prone to OS in the context of implantation. More interestingly, a combined treatment of two antioxidants, N-acetylcysteine (NAC) and α-tocopherol (αTCP), significantly attenuated paraquat-induced implantation failure in P_4-treated *Fkbp52*$^{-/-}$ mice (Table 3), indicating the contribution of OS to implantation failure. Our speculation that *Fkbp52*$^{-/-}$ mice are sensitive to OS is supported by the finding of higher levels of bound 8-isoprostane, a lipid peroxidation marker, in C57BL6/129 *Fkbp52*$^{-/-}$ uteri than in WT uteri on day 4 of pseudopregnancy (Fig. 3*B*).

***Fkbp52*$^{-/-}$ Mouse Embryonic Fibroblasts with Reduced PRDX6 Levels Are Susceptible to OS.** Because PRDX6 protects cells from membrane damage associated with phospholipid peroxidation, we speculated that reduced PRDX6 would reduce cell viability if challenged with overt OS. Indeed, in vitro studies with WT and *Fkbp52*$^{-/-}$ mouse embryonic fibroblasts (MEFs) show that FKBP52 deficiency is associated with reduced PRDX6 levels (Fig. 3*C*) and enhances H_2O_2-induced cell death (Fig. 3*D*). This adverse effect in *Fkbp52*$^{-/-}$ MEFs was reversed substantially by supplementation of NAC (Fig. 3*E*) and, more importantly, by forced expression of PRDX6 (Fig. 3 *E* and *F*), suggesting that *Fkbp52* deficiency lowers the threshold against reactive oxygen species (ROS) by reducing PRDX6 levels. Because PR expression is undetectable in these MEFs (Fig. S4), these results provide evidence for FKBP52's role independent of PR function.

Discussion

The highlight of the present study is that *Fkbp52*$^{-/-}$ uteri are susceptible to OS because of reduced PRDX6 levels. Although further investigation is warranted to explore the mechanism by which FKBP52 regulates PRDX6 levels, our observation of physical interaction between FKBP52 and PRDX6 suggests that FKBP52 stabilizes PRDX6 protein and attenuates its degradation as a function of its chaperone activity. FKBP52's roles in protein stability, folding, and trafficking have been reported previously (5–7).

The reduced tolerance to OS in *Fkbp52*$^{-/-}$ mice results in paraquat-induced failure of implantation and higher levels of ROS generation in the uterus. Because excess P_4 cannot prevent implantation failure in the face of overt OS induced by paraquat in CD1 *Fkbp52*$^{-/-}$ females, we believe that FKBP52 regulates OS, in addition to its function in optimizing PR activity and other potential functions. In fact, FKBPs have several physiological roles, including binding and sequestration of calcineurin, protein folding and assembly, protein trafficking, and direct regulation of protein activity (15). Our present study adds another function to the list of various activities that have been reported for FKBP52.

Table 1. Paraquat adversely affects implantation in *Fkbp52*$^{-/-}$ mice

Genotype	Paraquat (mg/kg)	No. of mice	No. of mice with IS (%)	No. of IS	No. of blastocysts recovered
WT	15	7	7 (100%)	12.1 ± 1.7	N/A
	20	7	7 (100%)	12.0 ± 0.7	N/A
Fkbp52$^{-/-}$ + P_4	0	8	8 (100%)	10.6 ± 0.6	N/A
	15	7	2 (29%)*	12.0 ± 2.3	25†
	20	5	1 (20%)*	5.0	17‡

WT and *Fkbp52* $^{-/-}$ females on a CD1 background were mated with CD1 WT fertile males, and the number of implantation sites (IS) was examined on day 5 of pregnancy. *Fkbp52*$^{-/-}$ females were treated with P_4 (2 mg/d) on days 2–4 of pregnancy. Paraquat was injected on day 4. Uteri without IS were flushed with saline to recover any unimplanted blastocysts. Values are mean ± SEM.
$^*P < 0.05$ compared with WT mice treated with the same dose of paraquat; Student's *t* test. N/A = not applicable.
†Twenty-five blastocysts were recovered from five mice.
‡Seventeen blastocysts were recovered from four mice.

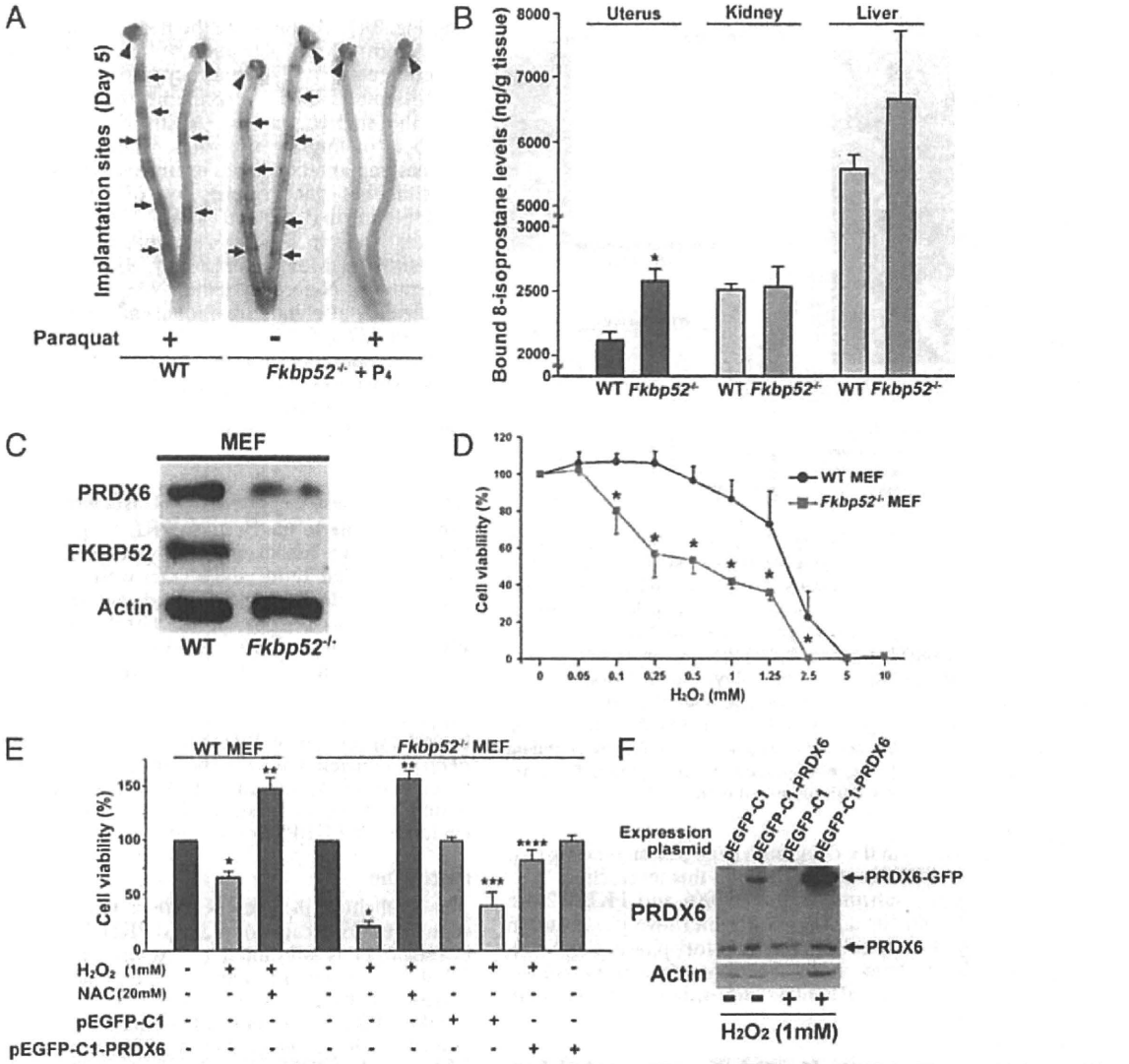

Fig. 3. *Fkbp52*$^{-/-}$ uteri are more prone to OS. (*A*) OS inducer paraquat blocks embryo implantation in P_4-primed CD1 *Fkbp52*$^{-/-}$ females on day 5 of pregnancy, whereas paraquat-treated CD1 WT uteri have normal numbers of implantation sites as demarcated by blue bands. *Fkbp52*$^{-/-}$ females were treated with P_4 (2 mg/d) on days 2–4 of pregnancy. Paraquat was injected on day 4. Arrows and arrowheads indicate implantation sites and ovaries, respectively. (*B*) Increased levels of bound 8-isoprostane, a lipid peroxidation marker, in C57BL6/129 *Fkbp52*$^{-/-}$ uteri on day 4 of pseudopregnancy. Values are mean ± SEM of three independent samples. *$P < 0.05$ compared with WT mice. (*C*) Decreased levels of PRDX6 in *Fkbp52*$^{-/-}$ MEFs. Actin was used as a loading control. (*D*) Heightened sensitivity of *Fkbp52*$^{-/-}$ MEFs to H_2O_2-induced OS. Cells were treated with different concentrations of H_2O_2 for 24 h, and cell viability was evaluated by MTT assay. Values are mean ± SEM of six replicates from three independent experiments. *$P < 0.05$ compared with WT mice. (*E*) H_2O_2-induced cell death in *Fkbp52*$^{-/-}$ MEFs is protected by addition of NAC and forced expression of PRDX6. Cell viability was evaluated by MTT assay. Values are mean ± SEM of six replicates from three independent experiments. *$P < 0.05$, compared with vehicle-treated cells derived from mice of the same genotype. **$P < 0.05$, compared with H_2O_2-treated cells derived from mice of the same genotype. ***$P < 0.05$, compared with *Fkbp52*$^{-/-}$ cells transfected with pEGFP-C1 control plasmids; ****$P < 0.05$ compared with H_2O_2-treated *Fkbp52*$^{-/-}$ cells with transfection of pEGFP-C1 control plasmids. (*F*) PRDX6-GFP fused protein is induced effectively by transfection of pEGFP-C1-PRDX6 plasmids in *Fkbp52*$^{-/-}$ MEFs. pEGFP-C1 is a control plasmid.

PRDX6 is a unique nonredundant antioxidant that acts independently of other PRDXs and antioxidant enzymes (10–12). A recent study shows that *Prdx6*-deficient (*Prdx6*$^{-/-}$) mice have normal development, but paraquat-induced OS causes abnormal phenotypes such as lower survival rate, again not resulting from changes in gene expression and/or activity of other antioxidant enzymes (12). Thus, PRDX6 might be a critical antioxidant against exogenous OS. Our present finding of increased susceptibility of *Fkbp52*$^{-/-}$ uteri to OS during implantation because of reduced PRDX6 levels underscores the importance of uterine FKBP52–PRDX6 signaling during the periimplantation period. Although *Prdx6*$^{-/-}$ females were reported to be fertile (12), it is possible that exposure to OS will impair fertility in these mice. Indeed, it is known that certain genes serve critical functions during physiologically altered conditions. For example, deficiency of prolactin (PRL)-like protein A (PLP-A), a nonclassical member of the PRL family expressed in the mouse placenta, has little effect on female fertility under normal conditions, but PLP-A mutants show compromised pregnancy when exposed to a stressor (16). Thus, fertility in *Prdx6*$^{-/-}$ females could be compromised if PRDX6 deficiency is superimposed with OS. Future studies are warranted to characterize the female fertility phenotype in *Prdx6*$^{-/-}$ mice in a more systematic manner under normal and OS conditions. Collectively, our observations suggest that implantation failure in *Fkbp52*$^{-/-}$ mice not only is caused by the reduced PR activity but also is compounded by increased OS levels.

There is evidence that smoking and alcohol consumption reduce fertility in women by elevating OS (17, 18). Evidence also indicates that dietary antioxidant and diet-related exposures to ROS affect the timing and maintenance of pregnancy (19). These

Table 2. Paraquat inhibits implantation of transferred WT blastocysts in *Fkbp52*$^{-/-}$ recipients

Genotype of blastocysts	Genotype of recipients	Paraquat (mg/kg)	No. of blastocysts transferred	No. of recipients	No. of mice with IS (%)	No. of IS (%)	No. of blastocysts recovered
WT	WT	15	77	6	6 (100%)	58/77 (75%)	N/A
WT	*Fkbp52*$^{-/-}$+P_4	15	60	5	1 (20%)	1/60 (2%)	30*

Day 4 CD1 WT blastocysts were transferred into uteri of CD1 WT or CD1 *Fkbp52*$^{-/-}$ recipients on day 4 of pseudopregnancy. *Fkbp52*$^{-/-}$ recipients were treated with P_4 (2 mg/d) on days 2–4 of pregnancy. Paraquat was injected into the recipients 5 h before embryo transfer on day 4 of pregnancy. Uteri without IS were flushed with saline to recover any unimplanted blastocysts. N/A, not applicable.
*Thirty blastocysts were recovered from four mice.

findings, together with our observation that commercial rodent diets influence uterine gene expression and the timing of implantation in mice (20), suggest the possibility of ROS-induced alterations in uterine functions related to implantation. Because *Prdx6* is expressed primarily in the stroma in WT uteri on day 4 of pregnancy, the reduction of stromal *Prdx6* in *Fkbp52*$^{-/-}$ uteri even with P_4 supplementation may attenuate stromal function more drastically when exposed to OS. *Hoxa10* and *Ihh* are expressed in the stroma and epithelium, respectively, in day 4 pregnant mouse uteri (21, 22). Our results show that paraquat down-regulates *Hoxa10* expression without altering *Ihh* expression in *Fkbp52*$^{-/-}$ uteri (Fig. S5). In this respect, stromal *Prdx6* could be more important in protecting the uterus from overt OS and allowing implantation to proceed. Interestingly, we found a similar expression pattern of PRDX6 and FKBP52 in human endometrium and higher expression of *Prdx6* during the secretory phase, suggesting that these proteins may have physiological roles in human endometrium and implantation. It will be interesting to see whether endometria from patients with recurrent implantation failure have higher ROS because of low PRDX6 levels.

During the periimplantation period, embryos are exposed to low oxygen tension (23). Because preimplantation embryos are sensitive to OS (24), it is believed that a low oxygen condition is conducive to normal embryonic growth and development. This notion is consistent with the finding that antioxidants prevent ROS-induced abnormal embryo growth in culture (25, 26). Thus, the embryonic environment facing excess OS interferes with successful implantation. It also is a distinct possibility that the uterine environment is hypoxic during the periimplantation period to protect embryos from OS. Our findings that WT, but not *Fkbp52*$^{-/-}$, pregnant females treated with paraquat have normal implantation suggest that the uterus has a built-in protective system to combat OS to a degree and that PRDX6 is a critical player in this system. With increased angiogenesis after implantation, oxygen tension in the uterus and placenta increases, gradually exposing the developing embryo to higher ROS levels. Because a major role of the deciduum and placenta is to accommodate and protect the growing embryos, our data showing strong expression of *Prdx6* in these tissues in WT mice suggest that decidual and placental PRDX6 has an antioxidant function and protects embryos against increased oxygen tension at that time.

Endometriosis, the growth of endometrium-like tissues outside the uterus, is a common gynecological disease often associated with pelvic pain and infertility (27). Accumulating evidence shows that OS is associated with the pathogenesis of endometriosis and endometriosis-related infertility including implantation failure (28). Because our recent study has shown that FKBP52 levels are down-regulated in endometria of women with endometriosis compared with women without endometriosis (29), reduced FKBP52 levels may lead to endometrial PRDX6 deficiency, increasing uterine susceptibility to ROS, aggravating endometriosis, and adversely affecting endometrial receptivity in patients with endometriosis.

In conclusion, we show here that uterine FKBP52–PRDX6 signaling is a key player against ROS during pregnancy, an intriguing finding regarding a role of FKBP52–PRDX6 in uterine biology in the context of implantation.

Materials and Methods

Mice. C57BL/6/129 and CD1 *Fkbp52*$^{-/-}$ mice (9, 30) and C57BL6/129 *Pgr*$^{-/-}$ mice (31) were used in this study. FKBP52 and PR mutant mice were originally obtained from David Smith (Mayo Clinic, Scottsdale, AZ) and Bert O'Malley (Baylor College of Medicine, Houston, TX), respectively. All protocols for the present study were reviewed and approved by the Cincinnati Children's Research Foundation Institutional Animal Care and Use Committee.

Analysis of Implantation and Blastocyst Transfer. Mice were examined for implantation as described previously (9). WT and *Fkbp52*$^{-/-}$ females (2- to 5-mo-old) were mated with WT fertile males to induce pregnancy (day 1 = vaginal plug). To supplement *Fkbp52*$^{-/-}$ females with exogenous P_4, they were given an s.c. injection of P_4 (2 mg/d, s.c.) on days 2–4 of pregnancy. For induction of OS, paraquat was given i.p. to WT or *Fkbp52*$^{-/-}$ mice on day 4 (0900 hours) of pregnancy. For antioxidant treatment, NAC (50 mg/kg body weight) and αTCP (1g/kg body weight) were given i.p. daily on days 2–4. Pregnant females were killed on day 5 (0900 hours), and implantation sites were evaluated by i.v. injection of a Chicago blue dye solution. Uteri without implantation sites were flushed with saline to recover any unimplanted blastocysts. For blastocyst transfer experiments, pseudopregnant recipients were generated by mating females with vasectomized males. Paraquat was injected into recipients 5 h before embryo transfer on day 4 (0700 hours) of pregnancy. Day-4 WT blastocysts were transferred into day 4 uteri of WT or *Fkbp52*$^{-/-}$ pseudopregnant recipients (1200 hours), and implantation sites were examined 24 h later (day 5, 1200 hours).

Treatment with P_4 and/or E_2. To assess the effects of ovarian hormones on uterine *Prdx6* expression, CD1 WT females were ovariectomized and rested for 2 wk. They then were given a single s.c. injection of P_4 (2 mg) and/or E_2 (100 ng) (32). The control group of mice received only the vehicle (oil). Mice were killed after 24 h, and uteri were collected for Northern and in situ hybridization.

Human Tissues. Endometrial tissues were obtained from 24 women who had shown regular menstrual cycles without any hormonal treatment for at least 6 months. Endometrial samples were dated according to the women's

Table 3. Reversal of paraquat-induced implantation failure by treatment of antioxidants

Genotype	Paraquat (2 mg/kg)	NAC + αTCP	No. of mice	No. of mice with IS (%)	No. of IS (mean ± SEM)	No. of blastocysts recovered
Fkbp52$^{-/-}$ + P_4	+	–	10	1 (10%)	13.0	35†
	+	+	8	5 (63%)*	6.2 ± 1.7	22‡

Mice were given an i.p. injection of paraquat on day 4 of pregnancy. P_4 (2 mg/d) was administrated s.c. into each CD1 *Fkbp52*$^{-/-}$ mouse on days 2–4. NAC (50 mg/kg) and α-tocopherol (αTCP) (1 g/kg) were injected i.p. on days 2–4. Mice were killed on day 5, and their IS were examined by the blue dye method.
*$P < 0.05$ compared with *Fkbp52*$^{-/-}$ mice treated with the same dose of paraquat, P_4; Student's *t* test.
†Thirty-five blastocysts were recovered from nine mice.
‡Twenty-two blastocysts were recovered from three mice. Dormant-looking blastocysts were recovered from mice in which blue bands were not present or were very weak.

menstrual history and standard histological criteria (33). The experimental procedures were approved by the institutional review board of the University of Tokyo, and signed informed consent for the use of tissues was obtained from each woman.

2D-DIGE Analysis and Protein Identification. WT, *Fkbp52*$^{-/-}$, and *Pgr*$^{-/-}$ mice on C57BL6/129 background were ovariectomized, rested for 2 wk, and then treated daily with P_4 (2 mg) for 2 d. Mice were killed 24 h after the second P_4 injection, and their uteri were collected and processed for 2D-DIGE. Proteins were extracted from uterine tissues from three independent WT and *Pgr*$^{-/-}$ mice and four *Fkbp52*$^{-/-}$ mice, and 2D-DIGE and protein identification were performed as previously described by us (*SI Materials and Methods*) (14).

Immunoblotting. Protein extraction and Western blotting were performed as described (14). Antibodies to PRDX6, FKBP52 (kindly provided by Marc B. Cox, University of Texas, El Paso, TX), and actin were used. Actin served as a loading control.

Immunohistochemistry. Immunostaining of PRDX6 was performed in formalin-fixed paraffin-embedded sections using a specific antibody to PRDX6 (kindly provided by Aron B. Fisher, University of Pennsylvania, Philadelphia).

In Situ Hybridization. Paraformaldehyde-fixed frozen sections were hybridized with ^{35}S-labeled cRNA probes as described (13).

Northern Hybridization. Northern blotting was performed as described previously (13). *Rpl7* served as a housekeeping gene.

Immunoprecipitation. Decidual cells were isolated as described previously (34). Protein lysates were immunoprecipitated with an anti-FKBP52 antibody, and complexes were run on SDS/PAGE and immunoblotted using antibodies specific to PRDX6 or FKBP52. The control immunoprecipitation was performed by incubating the lysates with rabbit IgG.

Quantitative PCR. Quantitative PCR was performed as previously described (29). A housekeeping gene *Gapdh* was used as an internal standard.

RT-PCR. RT-PCR was performed as previously described (14). *Actb* served as a housekeeping gene.

8-Isoprostane Assay. Tissue levels of 8-isoprostane were assayed as described previously (35).

Isolation and Culture of MEFs. WT and *Fkbp52*$^{-/-}$ MEFs (kindly provided by Marc B. Cox, University of Texas, El Paso, TX) were isolated as described previously (8). The cells were maintained in DMEM supplemented with 10% FBS and penicillin/streptomycin.

MTT Assays. MEFs were cultured for 24 h in DMEM containing various concentrations of H_2O_2, and cell viability was determined with MTT assay as described previously (Promega) (36). To examine the effects of NAC on H_2O_2-induced cell damage, MEFs were pretreated with NAC for 24 h and then were treated with H_2O_2. To examine the effects of PRDX6 on H_2O_2-induced cell damage, *Fkbp52*$^{-/-}$ MEFs were transiently transfected with pEGFP-C1 (control vector carrying GFP alone, Clontech) or pEGFP-C1-PRDX6 (carrying GFP-PRDX6 fusion construct) plasmids (kindly provided by Aron Fisher, University of Pennsylvania, Philadelphia, PA) by liposome transfection. The cells expressing GFP or PRDX6-GFP fusion proteins were incubated with H_2O_2 for 24 h.

Statistical Analysis. Statistical analyses were performed using two-tailed Student's *t* test and ANOVA as appropriate. $P < 0.05$ was considered statistically significant.

ACKNOWLEDGMENTS. We thank Erin L. Adams for editing the manuscript. Tissue 8-isoprostane levels were measured by the late Dr. Jason Morrow (Vanderbilt University, Nashville, TN) who died in 2008. We are very grateful for his contributions to our research. Anti-PRDX6 antibody and pEGFP-C1 and pEGFP-C1-PRDX6 plasmids were kindly provided by Dr. Aron Fisher (University of Pennsylvania, Philadelphia, PA). Anti-FKBP52 antibody and WT and *Fkbp52*$^{-/-}$ MEFs were kindly provided by Dr. Marc B. Cox (University of Texas, El Paso, TX). This study was supported in part by National Institutes of Health Grants HD12304 and DA006668. Y.H. is supported by the Japan Society for the Promotion of Science Postdoctoral Fellowships for Research Abroad. N.A. is supported by the 2214-Abroad Research Fellowship for PhD students from the Scientific and Technological Research Council of Turkey (TUBITAK).

1. Margalioth EJ, Ben-Chetrit A, Gal M, Eldar-Geva T (2006) Investigation and treatment of repeated implantation failure following IVF-ET. *Hum Reprod* 21:3036–3043.
2. Dey SK, et al. (2004) Molecular cues to implantation. *Endocr Rev* 25:341–373.
3. Lydon JP, et al. (1995) Mice lacking progesterone receptor exhibit pleiotropic reproductive abnormalities. *Genes Dev* 9:2266–2278.
4. Smith DF (2004) Tetratricopeptide repeat cochaperones in steroid receptor complexes. *Cell Stress Chaperones* 9:109–121.
5. Zhong L, et al. (2004) Heat-shock treatment-mediated increase in transduction by recombinant adeno-associated virus 2 vectors is independent of the cellular heat-shock protein 90. *J Biol Chem* 279:12714–12723.
6. Davies TH, Sánchez ER (2005) Fkbp52. *Int J Biochem Cell Biol* 37:42–47.
7. Mamane Y, Sharma S, Petropoulos L, Lin R, Hiscott J (2000) Posttranslational regulation of IRF-4 activity by the immunophilin FKBP52. *Immunity* 12:129–140.
8. Tranguch S, et al. (2005) Cochaperone immunophilin FKBP52 is critical to uterine receptivity for embryo implantation. *Proc Natl Acad Sci USA* 102:14326–14331.
9. Tranguch S, et al. (2007) FKBP52 deficiency-conferred uterine progesterone resistance is genetic background and pregnancy stage specific. *J Clin Invest* 117:1824–1834.
10. Manevich Y, Fisher AB (2005) Peroxiredoxin 6, a 1-Cys peroxiredoxin, functions in antioxidant defense and lung phospholipid metabolism. *Free Radic Biol Med* 38:1422–1432.
11. Phelan SA (1999) AOP2 (antioxidant protein 2): Structure and function of a unique thiol-specific antioxidant. *Antioxid Redox Signal* 1:571–584.
12. Wang X, et al. (2003) Mice with targeted mutation of peroxiredoxin 6 develop normally but are susceptible to oxidative stress. *J Biol Chem* 278:25179–25190.
13. Das SK, et al. (1994) Heparin-binding EGF-like growth factor gene is induced in the mouse uterus temporally by the blastocyst solely at the site of its apposition: A possible ligand for interaction with blastocyst EGF-receptor in implantation. *Development* 120:1071–1083.
14. Daikoku T, et al. (2005) Proteomic analysis identifies immunophilin FK506 binding protein 4 (FKBP52) as a downstream target of Hoxa10 in the periimplantation mouse uterus. *Mol Endocrinol* 19:683–697.
15. Kay JE (1996) Structure-function relationships in the FK506-binding protein (FKBP) family of peptidylprolyl cis-trans isomerases. *Biochem J* 314:361–385.
16. Ain R, Dai G, Dunmore JH, Godwin AR, Soares MJ (2004) A prolactin family paralog regulates reproductive adaptations to a physiological stressor. *Proc Natl Acad Sci USA* 101:16543–16548.
17. Hakim RB, Gray RH, Zacur H (1998) Alcohol and caffeine consumption and decreased fertility. *Fertil Steril* 70:632–637.
18. Howe G, Westhoff C, Vessey M, Yeates D (1985) Effects of age, cigarette smoking, and other factors on fertility: Findings in a large prospective study. *Br Med J (Clin Res Ed)* 290:1697–1700.
19. Ruder EH, Hartman TJ, Blumberg J, Goldman MB (2008) Oxidative stress and antioxidants: Exposure and impact on female fertility. *Hum Reprod Update* 14:345–357.
20. Wang H, et al. (2005) Variation in commercial rodent diets induces disparate molecular and physiological changes in the mouse uterus. *Proc Natl Acad Sci USA* 102:9960–9965.
21. Lim H, Ma L, Ma WG, Maas RL, Dey SK (1999) Hoxa-10 regulates uterine stromal cell responsiveness to progesterone during implantation and decidualization in the mouse. *Mol Endocrinol* 13:1005–1017.
22. Matsumoto H, Zhao X, Das SK, Hogan BL, Dey SK (2002) Indian hedgehog as a progesterone-responsive factor mediating epithelial-mesenchymal interactions in the mouse uterus. *Dev Biol* 245:280–290.
23. Fischer B, Bavister BD (1993) Oxygen tension in the oviduct and uterus of rhesus monkeys, hamsters and rabbits. *J Reprod Fertil* 99:673–679.
24. Dennery PA (2007) Effects of oxidative stress on embryonic development. *Birth Defects Res C Embryo Today* 81:155–162.
25. Nonogaki T, Noda Y, Narimoto K, Umaoka Y, Mori T (1991) Protection from oxidative stress by thioredoxin and superoxide dismutase of mouse embryos fertilized in vitro. *Hum Reprod* 6:1305–1310.
26. Wang X, et al. (2002) Vitamin C and vitamin E supplementation reduce oxidative stress-induced embryo toxicity and improve the blastocyst development rate. *Fertil Steril* 78:1272–1277.
27. Giudice LC, Kao LC (2004) Endometriosis. *Lancet* 364:1789–1799.
28. Augoulea A, Mastorakos G, Lambrinoudaki I, Christodoulakos G, Creatsas G (2009) The role of the oxidative-stress in the endometriosis-related infertility. *Gynecol Endocrinol* 25:75–81.
29. Hirota Y, et al. (2008) Deficiency of immunophilin FKBP52 promotes endometriosis. *Am J Pathol* 173:1747–1757.
30. Cheung-Flynn J, et al. (2005) Physiological role for the cochaperone FKBP52 in androgen receptor signaling. *Mol Endocrinol* 19:1654–1666.
31. Lydon JP, et al. (1995) Mice lacking progesterone receptor exhibit pleiotropic reproductive abnormalities. *Genes Dev* 9:2266–2278.
32. Lim H, et al. (1997) Multiple female reproductive failures in cyclooxygenase 2-deficient mice. *Cell* 91:197–208.
33. Noyes RW, Hertig AI, Rock J (1950) Dating the endometrial biopsy. *Fertil Steril* 1:3–25.
34. Hirota Y, et al. (2010) Uterine-specific p53 deficiency confers premature uterine senescence and promotes preterm birth in mice. *J Clin Invest* 120:803–815.
35. Morrow JD, Roberts LJ, 2nd (1999) Mass spectrometric quantification of F2-isoprostanes in biological fluids and tissues as measure of oxidant stress. *Methods Enzymol* 300:3–12.
36. Daikoku T, et al. (2007) Extracellular signal-regulated kinase is a target of cyclooxygenase-1-peroxisome proliferator-activated receptor-delta signaling in epithelial ovarian cancer. *Cancer Res* 67:5285–5292.

Research article

Death effector domain–containing protein (DEDD) is required for uterine decidualization during early pregnancy in mice

Mayumi Mori,[1] Miwako Kitazume,[1] Rui Ose,[2] Jun Kurokawa,[1] Kaori Koga,[3] Yutaka Osuga,[3] Satoko Arai,[1] and Toru Miyazaki[1]

[1]Laboratory of Molecular Biomedicine for Pathogenesis, Center for Disease Biology and Integrative Medicine, Faculty of Medicine, The University of Tokyo, Bunkyo-ku, Tokyo, Japan. [2]Department of Human Genome Research, Kazusa DNA Research Institute, Kisarazu, Chiba, Japan. [3]Department of Obstetrics and Gynecology, Faculty of Medicine, The University of Tokyo, Bunkyo-ku, Tokyo, Japan.

During intrauterine life, the mammalian embryo survives via its physical connection to the mother. The uterine decidua, which differentiates from stromal cells after implantation in a process known as decidualization, plays essential roles in supporting embryonic growth before establishment of the placenta. Here we show that female mice lacking death effector domain–containing protein (DEDD) are infertile owing to unsuccessful decidualization. In uteri of *Dedd*$^{-/-}$ mice, development of the decidual zone and the surrounding edema after embryonic implantation was defective. This was subsequently accompanied by disintegration of implantation site structure, leading to embryonic death before placentation. Polyploidization, a hallmark of mature decidual cells, was attenuated in DEDD-deficient cells during decidualization. Such inefficient decidualization appeared to be caused by decreased Akt levels, since polyploidization was restored in DEDD-deficient decidual cells by overexpression of Akt. In addition, we showed that DEDD associates with and stabilizes cyclin D3, an important element in polyploidization, and that overexpression of cyclin D3 in DEDD-deficient cells improved polyploidization. These results indicate that DEDD is indispensable for the establishment of an adequate uterine environment to support early pregnancy in mice.

Introduction

Approximately 10%–15% of couples experience infertility during their reproductive years, owing mainly to implantation failure. Among the reasons underlying such failure, defective development of functional decidua at the implantation site within the uterus has recently been highlighted (1–3). In response to implantation, stromal cells immediately surrounding the mucosal crypt where the embryo is embedded proliferate extensively and undergo differentiation into polyploid decidual cells, forming an avascular primary decidual zone, followed by a broad, well-vascularized secondary decidual zone. It is believed that this decidual structure is important for the provision of nutrition to the developing embryo and also acts as a barrier against uncontrolled trophoblast proliferation until the placenta develops. Analyses of mutant mice that show female infertility, such as in knockout mice for homeobox A10 (*Hoxa10*) (4, 5) or IL-11 receptor (6), have contributed to the investigation of the molecular mechanisms involved in decidualization. Recent evidence has implicated cell-cycle regulation as being essential for both the proliferation and differentiation of stromal cells. In particular, Das and colleagues reported that cyclin D3–dependent activation of cyclin-dependent kinase 4 (Cdk4) or Cdk6 appears to be involved sequentially in those two events during decidua formation (7). In addition to these essential elements, in this report, we present data indicating that the death effector domain–containing (DED-containing) protein DEDD is indispensable for the maturation of decidual cells and support of female fertility in mice.

We previously found that the DEDD protein, initially described as a member of the DED-containing protein family, is associated with the Cdk1/cyclin B1 complex, thereby decreasing the kinase activity of Cdk1 (8). This response impedes Cdk1-dependent mitotic progression, preserving synthesis of ribosomal RNA (rRNA) and protein and resulting in sufficient cell growth before cell division (8, 9). Consistently, depletion of DEDD results in a shortened mitotic duration, an overall decrease in the amount of cellular rRNA and protein, and decreased cell and body size (8, 9). In addition to the function of DEDD as a cell-cycle regulator, we recently determined that DEDD associates with S6K1 (10) and Akt (11), major elements of the signaling cascade involving mitogen-related PI3K. Such associations support the roles of S6K1 activity and Akt protein stability, respectively, in contributing to the maintenance of glucose homeostasis in the body (10, 11). Hence, DEDD is multifunctional and is involved in different physiological mechanisms. In fact, we found that female *Dedd*$^{-/-}$ mice are infertile, and embryos of all DEDD genotypes die during early pregnancy within the *Dedd*$^{-/-}$ uterus, whereas *S6K1*$^{-/-}$ female mice, which also show a similar small phenotype and attenuated glucose homeostasis, show normal fertility (12). Given the phenotypic similarity of *Dedd*$^{-/-}$ mice to other infertile mutant mice (4–6), this observation led us to address whether DEDD might also be involved in uterine decidualization.

In the present study, we assessed embryos implanted in *Dedd*$^{-/-}$ uteri. In addition, we analyzed the maturation state of uterine decidual cells from *Dedd*$^{-/-}$ mice in vitro and in vivo. We also studied the molecular mechanism underlying the inefficient decidualization of *Dedd*$^{-/-}$ cells.

Results

Female Dedd$^{-/-}$ *mice are infertile.* We found that *Dedd*$^{-/-}$ female mice exhibited complete sterility when mated with males of any genotype (*Dedd*$^{-/-}$, *Dedd*$^{+/-}$, or *Dedd*$^{+/+}$), although *Dedd*$^{-/-}$ offspring were born from the intercross of *Dedd*$^{+/-}$ mice at a Mendelian ratio, and

Conflict of interest: The authors have declared that no conflict of interest exists.
Citation for this article: *J Clin Invest.* 2011;121(1):318–327. doi:10.1172/JCI44723.

Table 1
Female *Dedd*$^{-/-}$ mice are infertile

Genotype		Offspring					
Female	Male	+/+	+/–	–/–	Sum	*n*	Birth rate
+/+	+/–	13 (46%)	15 (54%)	0 (0%)	28	6	4.67
+/+	–/–	0 (0%)	87 (100%)	0 (0%)	87	18	4.83
+/–	+/+	24 (51%)	23 (49%)	0 (0%)	47	10	4.70
+/–	+/–	108 (30%)	183 (51%)	66 (19%)	357	65	5.49
+/–	–/–	0 (0%)	47 (64%)	27 (36%)	74	17	4.35
–/–	+/+	0	0	0	0	23	0.00
–/–	+/–	0	0	0	0	37	0.00
–/–	–/–	0	0	0	0	12	0.00

The breeding efficiency in male-female combinations of various DEDD genotypes was investigated. Sum, total number of newborns; *n*, number of successful matings (with a vaginal plug); birth rate: sum/*n*.

Dedd$^{-/-}$ male mice were fertile (Table 1). Mating efficiency was comparable in female *Dedd*$^{-/-}$ mice and female mice of other genotypes, as assessed by vaginal plug formation (data not shown). The uterine *Dedd* mRNA level was upregulated after 4.5 dpc as assessed by quantitative RT-PCR (QPCR) (Figure 1A). An increase in *Dedd* expression was also observed in stromal cells differentiated to mature decidual cells in vitro in the presence of estrogen, progesterone (P4), and heparin-binding EGF-like growth factor (HB-EGF) (Figure 1B). Upregulation of *DEDD* expression along with the decidualization was also detected in human uterine stromal cells (Figure 1C). These results suggested that uterine DEDD is important after implantation and that the maturation of uterine decidual cells may be associated with DEDD expression.

Consistently, when 4.5-dpc uteri were analyzed with injection of blue dye (1% Chicago blue solution) (13), the number of implantation sites was comparable in *Dedd*$^{-/-}$ and *Dedd*$^{+/+}$ mice (6.8 ± 0.73 in *Dedd*$^{-/-}$ mice and 7.4 ± 0.40 in *Dedd*$^{+/+}$ mice; $n = 5$ each). In addition, the spacing and crowding of implanted embryos in the uterus was also similar in *Dedd*$^{-/-}$ and *Dedd*$^{+/+}$ mice (Figure 1D). Histologic analysis of 4.5-dpc *Dedd*$^{-/-}$ uteri revealed normal embryonic implantation (Figure 1E). No difference was observed in the size of the edematous region and the decidual zone, which are formed in response to implantation (Figure 1E). Immunostaining for COX-2, an implantation site marker (14), corroborated the finding of normal embryonic implantation in *Dedd*$^{-/-}$ and *Dedd*$^{+/+}$ uteri (Figure 1E). Similarly, the mRNA level for *Ptgs2/Cox2* was comparable in *Dedd*$^{-/-}$ and *Dedd*$^{+/+}$ uteri, as assessed by QPCR with total RNA isolated from implantation sites (data not shown). However, anatomical analysis showed that in *Dedd*$^{-/-}$ uteri, the number of living embryos decreased rapidly between 5.5 and 8.5 dpc (Figure 1F). At 9.5 dpc, the period of placenta formation, no living embryos were detected in *Dedd*$^{-/-}$ uteri (Figure 1F). During this period, living embryos in *Dedd*$^{-/-}$ uteri were of smaller size compared with those in *Dedd*$^{+/+}$ uteri, and the difference in average embryo size between these two groups became more prominent at later dpc (Table 2). Thus, whereas implantation occurred normally in *Dedd*$^{-/-}$ uteri, embryos showed growth defects and died by 9.5 dpc, before placenta formation. Note that serum levels of estrogen and P4, as well as mRNA levels for the receptor for each hormone (*Esr1* and *Pgr*, respectively) were similar in *Dedd*$^{-/-}$ and *Dedd*$^{+/+}$ females (Supplemental Figure 1; supplemental material available online with this article; doi:10.1172/JCI44723DS1). Preimplantation uterine histology was also comparable (Supplemental Figure 2). In addition, the proliferation of uterine epithelial and stromal cells as well as expression induction of genes such as *Vegf* and *Lif* in response to estrogen were similar in *Dedd*$^{-/-}$ and *Dedd*$^{+/+}$ ovariectomized mice (Supplemental Figure 3). In addition, histologic ovarian morphology, ovulation, and intrauterine fertilization were normal in *Dedd*$^{-/-}$ females (data not shown).

Defective decidualization and disintegrated structure of the implantation site in Dedd$^{-/-}$ *uteri.* Histological analysis of 5.5-dpc uteri showed that the size of the decidual zone was smaller in *Dedd*$^{-/-}$ compared with *Dedd*$^{+/+}$ mice (Figure 2A). This was confirmed by immunostaining for the decidua marker tissue inhibitor of metalloproteinase 3 (TIMP3) (quantification also shown in Figure 2A) (15). Consistent with these results, mRNA levels for various genes that are highly expressed in decidual cells were decreased in *Dedd*$^{-/-}$ compared with *Dedd*$^{+/+}$ uteri, as assessed by QPCR with total RNA isolated from implantation sites (Figure 2B). Of these, the expression level of P4-sensitive bone morphogenetic protein 2 (*Bmp2*) gene was compromised at 5.5 d.p.c in *Dedd*$^{-/-}$ uteri, whereas that of *Hoxa10*, upstream of *Bmp2* (5, 16, 17), was similar to that in *Dedd*$^{+/+}$ uteri. In addition to the decidual zone, the size of the edematous region surrounding the decidual zone was also decreased in *Dedd*$^{-/-}$ compared with *Dedd*$^{+/+}$ mice (Figure 2A), suggesting that vascular permeability might be reduced in *Dedd*$^{-/-}$ uteri.

Such attenuated development of the decidual zone in *Dedd*$^{-/-}$ uteri was accompanied by disintegrated structure of the implantation site at later phases of pregnancy. At 7.5 dpc, a large proportion of decidual cells exhibited a shrunken shape, and marked bleeding was detected at the edge of the cavity in *Dedd*$^{-/-}$ uteri (Figure 2C). In 8.5-dpc *Dedd*$^{-/-}$ uteri, the structure of the outer wall of the embryonic cavity, which is supported by Reichert's membrane and trophoblastic giant cells (TGCs), had collapsed (Figure 2C), and irregular distribution of TGCs (i.e., invasion of TGCs into inner area of uteri) was more remarkable (Figure 2D). Such inadequate uterine environment may cause infertility in female *Dedd*$^{-/-}$ mice.

Defective polyploidy in Dedd$^{-/-}$ *decidual cells.* We next assessed the state of polyploidy, a hallmark of mature decidual cells, in *Dedd*$^{-/-}$ and *Dedd*$^{+/+}$ uterine stromal cells undergoing decidualization in vitro in the presence of estrogen, P4, and HB-EGF. As shown in Figure 3A, at days 3 and 7, the proportion of multinuclear cells observed microscopically was more than 50% smaller in *Dedd*$^{-/-}$ cells than in *Dedd*$^{+/+}$ cells. Consistent with this result, analysis of these cells by the flow cytometer after DNA staining revealed a significant decrease in the proportion of cells that possessed more than 4 copies of genomic DNA (indicated as 4n and 8n) in *Dedd*$^{-/-}$ compared with *Dedd*$^{+/+}$ cells (Figure 3B). Similar results were obtained in vivo in cells isolated from 4.5-dpc implantation sites in *Dedd*$^{-/-}$ and *Dedd*$^{+/+}$ uteri by collagenase treatment (Figure 3C). Thus, the defect in decidualization observed in *Dedd*$^{-/-}$ uteri was associated with attenuated terminal maturation with less polyploidy.

In contrast, the proliferative status of uterine stromal cells in response to implantation was not different in *Dedd*$^{-/-}$ and *Dedd*$^{+/+}$ mice, as judged by the comparable cell number isolated from implantation sites at 4.5 dpc ($1.08 \times 10^6 \pm 0.15 \times 10^6$ in *Dedd*$^{-/-}$

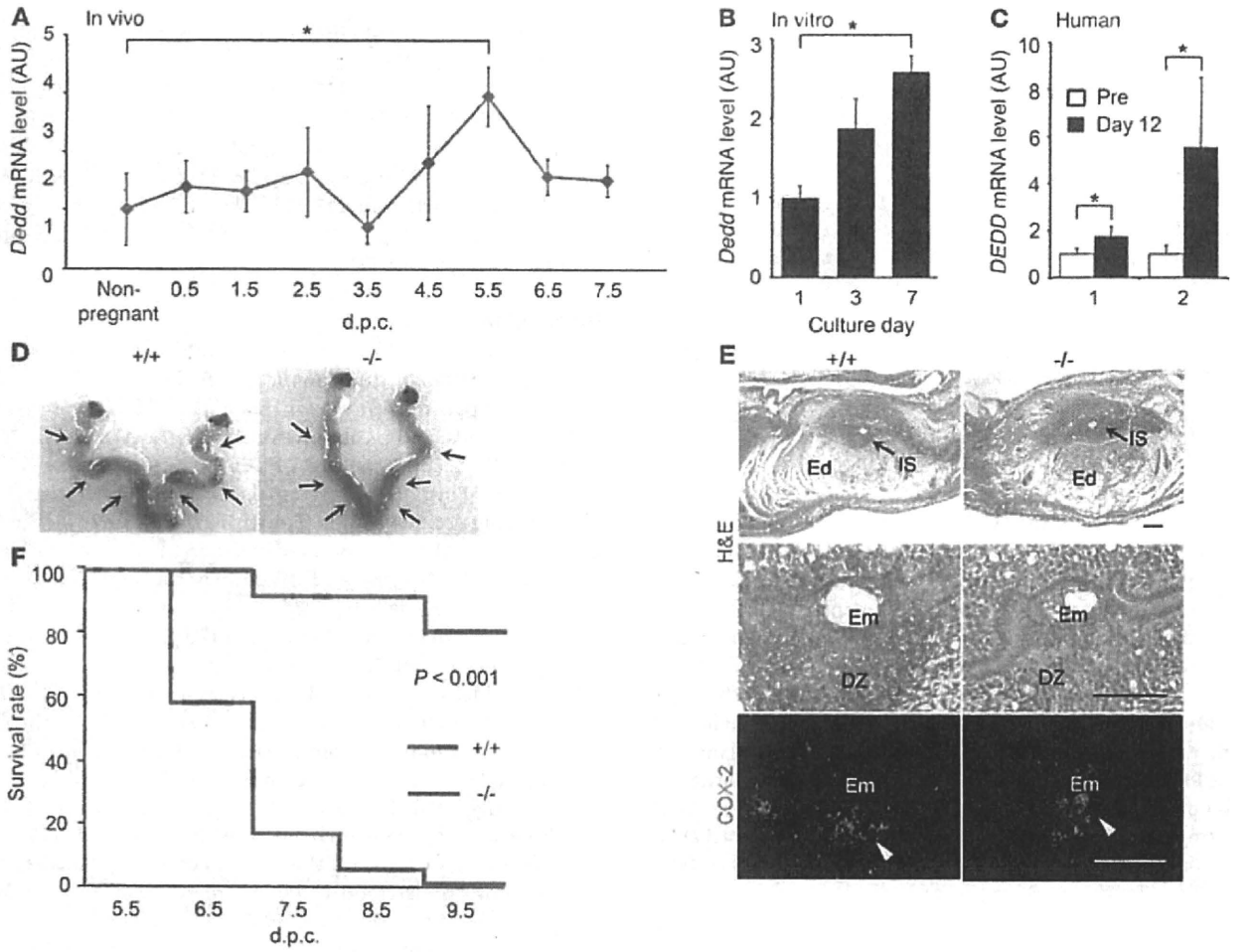

Figure 1

Postimplantation embryonic death in *Dedd*$^{-/-}$ uteri. (**A–C**) Increase in *Dedd* mRNA level in response to implantation in wild-type mouse (**A**) or in vitro decidualization in mouse uterine stromal (**B**) and human endometrial (**C**) cells, assessed by QPCR. Values were normalized to those of β-*actin* or *GAPDH* and are presented as relative expression to those of nonpregnant (**A**), day 1 (**B**), or undifferentiated (**C**) controls. Pre, undifferentiated cells; Day 12, decidualized cells at 12 days after the differentiation induction. In **C**, results from triplicate experiments using specimens from two individuals (1 and 2) are shown. Error bars indicate SEM. (**D**) Embryo spacing and crowding were assessed by blue dye injection. Representative photos of the uteri are shown. (**E**) Histologic analysis of implantation sites at 4.5 dpc in *Dedd*$^{+/+}$ (+/+) and *Dedd*$^{-/-}$ (–/–) uteri. Sections were stained with H&E or immunostained for COX-2. Em, embryo; DZ, decidual zone; Ed, edematous region (outside of DZ, white zone). Positive signals for COX-2 are indicated by arrowheads. Scale bars: 200 μm. (**F**) Survival rates of embryos during early gestation (Kaplan-Meier method). When embryo bodies were observed, regardless of size, they were regarded as "alive," whereas degenerated masses or those with scars at implantation sites were regarded as "dead." $n = 75$ for *Dedd*$^{+/+}$ and $n = 44$ for *Dedd*$^{-/-}$ uteri; log-rank, $\chi^2 = 13.2$. $^*P < 0.05$.

mice and $1.21 \times 10^6 \pm 0.075 \times 10^6$ in *Dedd*$^{+/+}$ mice; $n = 3$ each). Consistent with this result, when decidualizing stromal cells were challenged in vitro with 5-ethynil-2'-deoxyuridine (EdU; a nucleotide analog of thymidine), the proportion of EdU-incorporated cells was equivalent in *Dedd*$^{-/-}$ and *Dedd*$^{+/+}$ cells (Supplemental Figure 4A). Also, in vivo, 5.5-dpc implantation sites in *Dedd*$^{-/-}$ and *Dedd*$^{+/+}$ uteri stained similarly for Ki67, which identifies proliferating cells (Supplemental Figure 4B).

Decreased Akt level in Dedd$^{-/-}$ *uteri and increase in polyploidy by Akt expression in Dedd*$^{-/-}$ *decidual cells.* As we reported previously, the amount of Akt (all isotypes) is decreased in various *Dedd*$^{-/-}$ tissues, owing to decreased Akt protein stability (11). Notably, implantation sites in 5.5-dpc *Dedd*$^{-/-}$ uteri also showed decreased levels of Akt protein compared with those in *Dedd*$^{+/+}$ uteri, as assessed by immunoblotting with a pan-Akt antibody (Figure 4A). Parallel results were also obtained using in vitro decidualizing cells (Supplemental Figure 5). Signal for activated Akt phosphorylated at Thr308 was also decreased (Figure 4A, p-Akt). As we observed in mouse embryonic fibroblasts (MEFs) and other tissues (11), mRNA levels for *Akt1* and *Akt2* did not decrease in these cells (data not shown). To test whether the decrease in Akt protein was essential for the defect in polyploidy observed in *Dedd*$^{-/-}$ decidual cells (Figure 3), Akt-1 was overexpressed in in vitro differentiating *Dedd*$^{-/-}$ uterine stromal cells, and polyploidy was analyzed. As expected, the proportion of polynuclear cells was significantly increased by forced Akt-1 expression (Figure 4B). Thus, a decrease in Akt protein level appeared to be responsible for the inefficient decidualization observed in *Dedd*$^{-/-}$ uteri.

Table 2
Embryo size within *Dedd*$^{+/+}$ and *Dedd*$^{-/-}$ uteri

	Maternal genotype	Embryo size (mm^3)	*n*
Day 5.5	+/+	0.0059 ± 0.0014	9
	−/−	0.0039 ± 0.0012[A]	9
Day 6.5	+/+	0.17 ± 0.014	5
	−/−	0.044 ± 0.0096[B]	12
Day 7.5	+/+	0.51 ± 0.070	19
	−/−	0.25 ± 0.099[A]	11
Day 8.5	+/+	>5.00	11
	−/−	1.00 ± 0.33	7

Both *Dedd*$^{+/+}$ (+/+) females and *Dedd*$^{-/-}$ (−/−) females were mated with *Dedd*$^{+/+}$ males. Therefore, embryos in *Dedd*$^{+/+}$ uteri were either *Dedd*$^{+/-}$ or *Dedd*$^{+/+}$, whereas those in *Dedd*$^{-/-}$ uteri were all *Dedd*$^{+/-}$. There was no significant difference in the size among the *Dedd*$^{+/-}$ and *Dedd*$^{+/+}$ embryos in *Dedd*$^{+/+}$ uteri. [A]$P < 0.05$, [B]$P < 0.001$.

Dedd associates with cyclin D3 and supports its protein stability. Of the multiple functions of Akt, control of the cell cycle via regulation of D-type cyclins in terms of gene expression, protein stability, and localization within the cell has been documented in different physiologic and pathologic situations (18). Das and colleagues recently implicated cyclin D3 as a key regulator of polynuclearization (7, 19, 20). In addition, García-Morales et al. showed that the protein stability of cyclin D3 is downregulated by rapamycin, an inhibitor of mammalian target of rapamycin (mTOR), downstream of Akt in the PI3K signaling pathway (21). This suggests that the decrease in Akt protein in the absence of DEDD might influence cyclin D3, resulting in a defect in polyploidy. To test this, we stained *Dedd*$^{-/-}$ and *Dedd*$^{+/+}$ uteri for cyclin D3 at 5.5 dpc. As shown in Figure 5A, *Dedd*$^{-/-}$ decidua harbored fewer cyclin D3–positive cells. This decrease in cyclin D3 was confirmed by immunoblotting (Figure 5B). However, the mRNA level for cyclin D3 was similar in *Dedd*$^{-/-}$ and *Dedd*$^{+/+}$ uteri at 5.5 d.p.c (Figure 5C), suggesting that the stability of cyclin D3 is affected in *Dedd*$^{-/-}$ cells. Therefore, we measured the half-life of cyclin D3 protein in in vitro differentiating stromal cells at day 3. Importantly, the amount of cyclin D3 protein started to decrease within 30 minutes in *Dedd*$^{-/-}$ cells but not in *Dedd*$^{+/+}$ cells (Figure 5D). By 90 minutes, the protein level of cyclin D3 was more than 3-fold lower in *Dedd*$^{-/-}$ compared with *Dedd*$^{+/+}$ cells (Figure 5D). The presence of MG132, a proteasome inhibitor, tempered the decrease observed in *Dedd*$^{-/-}$ cells (Figure 5D). Thus, lack of DEDD resulted in instability of cyclin D3. As in the case of Akt, increase in cyclin D3 protein by overexpression improved polyploidy in *Dedd*$^{-/-}$ decidual cells (Figure 5E), indicating that a decrease in cyclin D3 protein level also appeared to be involved in the inefficient decidualization observed in *Dedd*$^{-/-}$ uteri.

Such a relationship among DEDD, cyclin D3, and Akt was also supported by an in situ mRNA analysis using 5.5- and 7.5-dpc *Dedd*$^{+/+}$ uteri, which demonstrated coexpression of these 3 genes at the decidual zone cells in vivo (Figure 6A). Furthermore, DEDD associated with cyclin D3. This is similar to our previous observations that DEDD binds to various proteins such as cyclin B1, S6K1, and Akt (8–11). As shown in Figure 6B, immunoprecipitation in HEK293T cells expressing both FLAG-tagged cyclin D3 and hemagglutinin-tagged (HA-tagged) DEDD showed that the two proteins coprecipitated, indicating that DEDD may facilitate a complex with cyclin D3. Therefore, DEDD might support the stability of cyclin D3 by two independent pathways: maintenance of the Akt protein level and direct formation of a DEDD/cyclin D3 complex. HA-tagged DEDD also coprecipitated with FLAG-tagged Cdk4 and Cdk6 (Figure 6B). Endogenous DEDD was also coprecipitated with cyclin D3, Cdk4, or Cdk6, when tested using protein isolated from implantation sites of 5.5-dpc uteri (Figure 6C). Similar to our observation that DEDD associates with Cdk1/cyclin B1 via direct binding to cyclin B1, DEDD might form a complex with Cdk4/cyclin D3 and Cdk6/cyclin D3, both of which are essential for the regulation of decidualization (9), via a direct association with cyclin D3.

Discussion

A new role for DEDD in uterine decidualization and female fertility. Results of the present study implicate DEDD as an indispensable element in supporting early pregnancy. First, DEDD was expressed in decidual cells, and its absence decreased the Akt protein level in these cells. Second, the lack of DEDD decreased the stability of cyclin D3. Third, *Dedd*$^{-/-}$ stromal cells showed defective polyploidy during decidualization. Fourth, in *Dedd*$^{-/-}$ uteri, inefficient polyploidy disturbed development of the decidual zone, which was accompanied by disintegrated structure of the implantation site. As a result of these defects, *Dedd*$^{-/-}$ uteri cannot support embryonic growth before the development of the placenta, resulting in complete infertility of *Dedd*$^{-/-}$ female mice.

The decidual cell polyploidy, which is a hallmark of mature decidual cells particularly in mice, is characterized by the formation of large mono- or binucleated cells, consisting of DNA with multiples of the haploid complement (22–24). Although it has been suggested that various biological processes including metabolic activity are associated with the polyploidy (25), the physiological significance of this event in uterine decidualization remains poorly understood. Complete infertility in female *Dedd*$^{-/-}$ mice whose decidua showed a normal proliferative activity but less polyploidy may suggest the functional importance of polyploidy for the support of embryonic growth during early pregnancy.

It could be argued that the general effect of DEDD deficiency, such as decreased body size and mild attenuation of insulin production (8–11), might cause infertility. However, this is unlikely, given that female *S6K1*$^{-/-}$ mice, which show a similar (or even more advanced) phenotype regarding body size and insulin production, remain fertile (12). Similarly, although *Akt1*$^{-/-}$ mice also showed fetal growth impairment due to placental inefficiency, adult females are fertile (26).

Association of DEDD with decidual polyploidy via support of Akt and cyclin D3 stability. One reason why the absence of DEDD causes infertility appears to be the decrease in the amount of Akt protein in uterine stromal/decidual cells. Recent evidence in humans and mice suggests that Akt may play a role in the regulation of decidualization and in the survival of decidual cells. Of note, Hirota et al. showed increased decidual polyploidy with upregulation of Akt phosphorylation in mice with deficiency for p53 restricted to the uterus (27). As we reported previously, DEDD forms a complex with Akt and heat shock protein 90 (Hsp90) and stabilizes all isoforms of Akt protein (11). It is possible that defective protein stability of cyclin D3 may be brought about, in part, by a decrease in Akt, based on the facts that D-type cyclins are substrates for Akt, cyclin D3 is regarded as a major regulator of polyploidy, and the deficient polyploidy observed in *Dedd*$^{-/-}$ cells was improved by forced expression of Akt-1. Nevertheless, the precise machinery whereby Akt influences the stability of cyclin D3 is not yet clear.

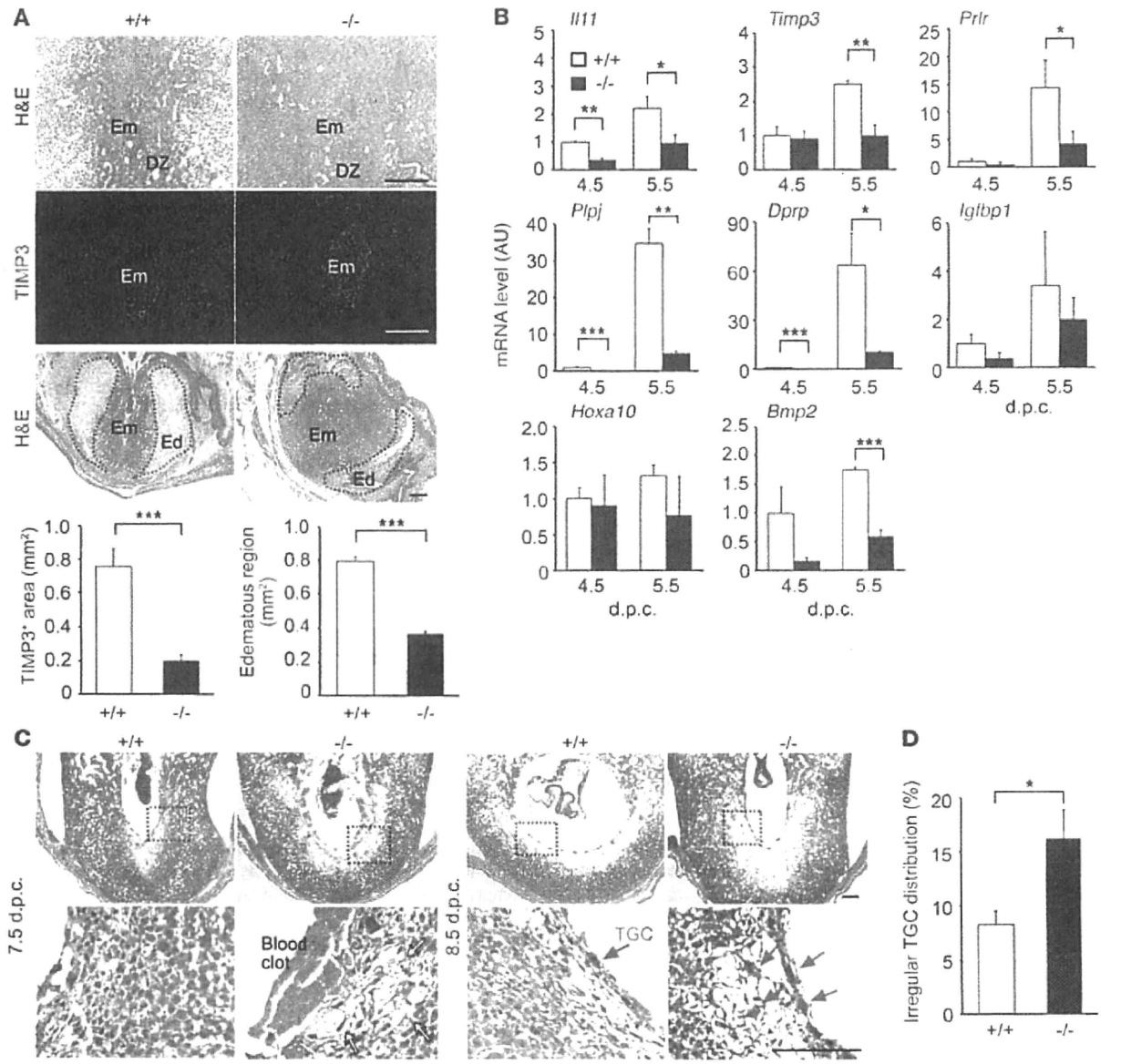

Figure 2

Defective decidualization in *Dedd*$^{-/-}$ uteri. (**A**) Implantation sites of 5.5-dpc *Dedd*$^{+/+}$ and *Dedd*$^{-/-}$ uteri were stained with H&E or immunostained for TIMP3. Scale bars: 200 μm. Quantification of decidual zone (TIMP3-positive area) and edematous region is also presented. At least 10 different sections in 3 different implantation sites were analyzed for each. Error bars indicate SEM. (**B**) mRNA levels of various genes that are highly expressed in decidua were analyzed by QPCR with total RNA isolated from 3 different implantation sites at 4.5 or 5.5 dpc. Values were normalized to those of β-*actin* and are presented as relative expression to 4.5-dpc *Dedd*$^{+/+}$ mice. Error bars indicate SEM. *Prlr*, prolactin receptor; *Plpj*, prolactin-like protein J; *Dprp*, decidual prolactin-related protein; *Igfbp1*, IGF-binding protein 1. (**C**) Histologic analysis of 7.5- and 8.5-dpc uteri (H&E staining). Higher magnification of the boxed area in the respective upper panel is presented in the lower panel. Arrows at 7.5 dpc indicate shrunken cells in *Dedd*$^{-/-}$ uterus. TGCs are denoted by blue arrows. Scale bars: 200 μm. (**D**) Irregular distribution of TGCs in *Dedd*$^{-/-}$ uterus. TGC numbers at the antimesometrial region of implantation sites were determined microscopically. At least 10 sections from 3 different specimens were examined. Data are shown as relative proportion of TGCs showing irregular distribution (invasion into the inner area). Error bars indicate SEM. $^{*}P < 0.05$, $^{**}P < 0.01$, $^{***}P < 0.001$.

Further studies are required to address the molecular mechanism. Interestingly, DEDD associates with cyclin D3; this might contribute structurally to the protein stability of cyclin D3.

Because cyclin D3–deficient mice do not show complete infertility, as observed in *Dedd*$^{-/-}$ mice (19, 28), a combination of various defects at the implantation site in addition to inefficient polyploidy — such as inadequate development of the edematous region (Figure 2A) and disintegrated structure of the implantation site at 7–8 d.p.c (Figure 2C) — might contribute to the overall infertility observed in *Dedd*$^{-/-}$ mice. These defects may also result from the decreased Akt level, given that Akt has diverse functions, including the maintenance of vascular permeability and an